University of Bath

Alternative formats
If you require this document in an alternative format, please contact:
openaccess@bath.ac.uk

1   **MINIMUM-MASS OPTIMISATION FOR HIGH-RATE MANUFACTURE OF DAMAGE**

2   **TOLERANT AND UNBUCKLED COMPOSITE COMPONENTS**

3   C. Scarth[a,*], M.W.D Nielsen[a], A.T. Rhead[a], R. Butler[a]

4   [a]Materials and Structures Centre, Department of Mechanical Engineering, University of Bath, Claverton Down,

5   Bath, United Kingdom, BA2 7AY

6   Email: C.Scarth@bath.ac.uk, M.W.D.Nielsen@bath.ac.uk, A.T.Rhead@bath.ac.uk, R.Butler@bath.ac.uk.

7   **ABSTRACT**

8   A significant increase in the rate of composite manufacture is needed to meet demand for short-range

9   commercial aircraft. The enabling automated manufacturing processes can, however, induce undesirable process

10   features such as wrinkles. Additionally, the potential for Barely Visible Impact Damage has resulted in

11   widespread use of overly-conservative strain allowables which has led to overweight aircraft structures.

12   Two new constraints are presented which enable formability and damage tolerance to be incorporated into a

13   two-stage minimum-mass optimisation framework for performance and manufacturability. An efficient,

14   approximate method is presented for determining a conservative lower bound on the strain required to propagate

15   a single, circular delamination, given a general through-thickness position and an upper bound on delamination

16   size. A Compatibility Index is used to predict the propensity for wrinkles to occur during a forming

17   manufacturing process.

18   Optimised stacking sequences for two benchmark design problems; a flat plate and blade-stiffened panel,

19   are obtained subject to minimum formability, damage tolerance and buckling constraints alongside common

20   industry design rules. The damage tolerance and formability constraints are met for a diverse set of design

21   requirements, without increasing mass or reducing buckling load, thereby demonstrating that components may

22   be optimised for manufacture using high-rate processes without detriment to performance.

23   **KEYWORDS**: Optimisation; Forming; Damage Tolerance; Buckling; Composite Materials; Design for

24   Manufacture

---

* Corresponding author

1. INTRODUCTION

Significant increases in the deposition rates of composites manufacturing technologies are required to meet demand for the next generation of short-range commercial aircraft. This increased production rate cannot compromise safety by introducing defects or process features, or sacrifice the capabilities of cured structures through added weight-penalty. Design processes must therefore be adapted to account for both manufacturability and performance to facilitate rollout of high-rate manufacturing technologies. Towards this end, this paper presents two new constraints for application during numerical optimisation: the first is an approximate figure of the relative merits of different stacking sequences in terms of tolerance to delaminations arising from Barely Visible Impact Damage (BVID), the second is a measure of the formability of preform stacks. In both instances, emphasis is placed upon simplified models which may be evaluated rapidly.

The potential for BVID to arise during service poses a significant risk of reducing the strength of laminated composites through formation of cracks and delaminations, which can propagate under subsequent loading. Current aircraft certification requirements dictate that BVID should not grow under ultimate load conditions (once in a lifetime with a factor of safety). Industrial strength limits are imposed using strain allowables, currently determined by coupon testing of laminates containing BVID. Due to the number of potential stack configurations it is, however, impractical to account for new design concepts such as non-standard ply angles or variations in stacking sequences using such coupon tests to derive these allowables. Recent efforts to model failure of impacted laminates have typically focussed on high-fidelity Finite Element (FE) simulations [1–3]. Such methods are capable of capturing precise damage morphologies and failure modes, however, require prohibitively high computation time. Reducing computation time when modelling damage embedded within larger structures is therefore important. Approaches such as the global-local method used to model delamination growth in stiffened panels in [4] can, for example, enable use of fine three-dimensional meshes for simulating delamination growth alongside more computationally efficient, coarsely-meshed shell models for predicting the global response.

Alternatively, simplified analytical approximations may be used to ensure computation times commensurate with design and optimisation applications. One potential mechanism for damage propagation, which is often critical for near back-face delaminations, is opening of delaminations arising from buckling of the thin sub-laminate created by the delamination under compressive loading. Following work by Chai and Babcock [5,6]

1 and other early work reviewed in [7], the authors recently updated their previous work [8,9] to create a simple

2 two-dimensional analytical model for this failure mechanism by approximating delaminations as ellipses [10].

3 This method uses VICONOPT [11], an efficient software using finite strip theory for design and analysis of

4 prismatic assemblies of laminated plates, to model sub-laminate buckling above an elliptical delamination

5 alongside analytical Mode I fracture expressions. This approach was shown to achieve good agreement with

6 experimental tests using artificially induced delaminations. A similar method was recently developed by Köllner

7 et al using a Rayleigh Ritz formulation for sub-laminate buckling around an elliptical boundary combined with a

8 mixed-mode criterion [12]. These two approaches were recently compared alongside nonlinear finite element

9 analysis and experimental tests in [13], to verify the suitability of the simplifying assumptions associated with

10 the Mode I-based criterion of [10] for design, and to ensure these assumptions are conservative in comparison to

11 a mixed-mode criterion. A key consideration when modelling panels containing delaminations is the

12 dependence of compressive behaviour upon delamination size and through-thickness location, as investigated in

13 [14]. As neither quantity is known during the design phase, it is important to identify critical, limiting values for

14 use in design.

15   An increased rate of manufacture of composite components may be achieved by forming stacks of multiple

16 plies simultaneously, into the required geometries, using automated processes. If both intra-ply shear and inter-

17 ply slip are constrained during this forming, compressive forces can arise in fibres leading to undesirable

18 wrinkling [15,16]. For a given geometry, stack formability, here defined as the capacity to undergo large in-

19 plane forming strains without wrinkling, can be affected by process parameters such as temperature and pressure

20 [17]. Ply interfaces can also be manipulated to selectively promote or inhibit inter-ply slip to prevent wrinkling

21 [18]. Notably, stacking sequence has been shown to strongly influence formability [19–21], as interactions

22 between fibres in adjacent plies can restrict shear and cause wrinkling if slip is impeded by friction at ply

23 interfaces [15,16].

24   The dependence of forming deformations upon individual ply orientations may be efficiently modelled

25 using kinematic techniques such as the pin-jointed net method [22], however, such techniques cannot capture

26 interactions between multiple plies, which are crucial for wrinkle formation. More accurate simulation of

27 multiple-ply stacks may be achieved using finite element software such as commercial forming packages

28 AniForm [15,16,23] and PAMFORM [24,25], or user-defined properties in general purpose software such as

29 ABAQUS or LS-DYNA [26]. These methods are, however, computationally expensive due to the number of

elements required to simulate wrinkle-scale deformations [16]. Recently, Johnson et al. [27] proposed a

Compatibility Index, a rapid analytical metric for laminate formability based upon the scalar products of

eigenvectors representing low-energy deformation modes of adjacent plies, achieving excellent correlation with

experimental forming trials. This method provides a suitable means of accounting for wrinkle formation within

stacking sequence optimisation, which is not currently achievable using less efficient methods.

Stacking sequence optimisation of composite structures can be challenging as laminate stiffness is a highly

nonlinear function of the ply orientations, which can cause gradient-based solvers to converge to local

optima [28]. Global search methods such as genetic algorithms (GAs) are consequently often used to optimise

ply orientations [29–33], however, such methods typically require a large number of model evaluations before

converging and do not guarantee a global optimum. These difficulties may be overcome by instead optimising

lamination parameters, an alternative representation of laminate stiffness originally proposed by Tsai et al.

[34,35]. This approach, initially developed by Miki et al. [36,37] and Fukunaga et al. [38,39], is advantageous as

laminate stiffness may be represented using a maximum of twelve lamination parameters regardless of the

number of plies. Additionally, laminate stiffness is a linear function of these parameters, thus simplifying the

relationship between objectives and constraints, and the design variables.. Mapping optimised lamination

parameters onto a practical stacking sequence requires solution of a nonlinear inverse problem. It is therefore

common to employ a two-stage design framework [40–42] using efficient gradient-based solvers to optimise

lamination parameters according to structural requirements, and genetic algorithms to solve the relatively

inexpensive problem of finding a stacking sequence which closely matches these parameters. Note that this

review is not intended to be exhaustive. The interested reader is referred to [43] for a comprehensive review of

recent developments in optimisation using lamination parameters and related methods.

Also noteworthy is the polar method presented by Vannucci and Verchery [44,45], wherein true invariants

of a general planar tensor are used as an alternative compact representation of the laminate stiffness and

anisotropy at the macroscopic scale. For instance, a fourth-order elasticity-like tensor may be defined using five

independent polar parameters. A multi-scale, two-level optimisation strategy, building upon the polar method,

has recently been developed by Montemurro et al. [46–49]. In the first stage, geometric features and polar

parameters are optimised for structural considerations such as mass, buckling load, strength, and manufacturing

requirements. The aim of the second stage is to find at least one stacking sequence to meet the optimised

geometric and polar parameters for each laminate within the structure, without restriction upon the stacking

sequence. This method has been applied to a wide range practical design problems considering both constant [47–49] and variable stiffness [46] laminates.

In this paper, the compression after impact model from [10,13] and Compatibility Index from [27] are expanded upon to develop two novel optimisation constraints for damage tolerance and formability respectively. An efficient search method is proposed for determining critical values of delamination size and through-thickness location, to estimate a lower bound on the strain required to cause delamination propagation, which is in turn used as a damage tolerance constraint. An integer linear programming method is proposed for efficiently evaluating the Compatibility Index, enabling its use as a formability constraint. These new constraints are presented in sections 2 and 3 respectively. Expressions for the lamination parameters are introduced in Section 4. The new damage tolerance and formability constraints are subsequently embedded within the commonly-used two-stage lamination parameter-based optimisation framework [40,42]. The primary purpose of this exercise is to demonstrate simultaneous consideration of manufacturing and performance-based design criteria, as evaluated using the new constraints, within an existing optimisation framework. Lamination parameters and thicknesses of finite element models are initially minimised subject to buckling and strain constraints. In the second stage, a stacking sequence is found to match the optimum lamination parameters while satisfying the new formability and damage tolerance constraints, thereby incorporating these figures of merit into laminate design. This framework is applied to example plate and blade stiffened panel models in Section 5 to demonstrate how aerospace structures may be designed for manufacture using high-rate processes, without detriment to performance, with results discussed in Section 6.

2. DAMAGE TOLERANCE METRIC

2.1. Overview

A significant risk of strength reduction in laminated composites may arise when in-service damage leads to cracking and delamination, and subsequent loading results in modes which force the stiff carbon fibres apart, propagating as cracks in the matrix. For instance, compressive failure modes of plates containing a delamination include symmetric closing, antisymmetric shearing, or symmetric opening, as shown in Figure 1. In the case of the latter, residual strength can be limited by growth in this opening mode due to buckling of the thin sub-laminate . Such opening can dominate, particularly when impact damage to flat panels results in larger delaminations near the back face [50], noting that the back face corresponds to the upper surface in Figure 1.

5

1   A two-dimensional analytical model was previously derived [10] for determining strains required to

2   propagate elliptical delaminations with known dimensions, arising at a specified ply interface, via the opening

3   mode shown in Figure 1c). This methodology was compared against a more-comprehensive model comprising

4   other modes of delamination propagation in [13], alongside nonlinear finite element analysis and experimental

5   tests. Although the simplified model [10] was found to be conservative, it adequately predicted relative trends in

6   the damage tolerance of different stacking sequences, and as such, its use in design applications was considered

7   justified by its relatively low computational cost. In this Section, this method is extended to eliminate the

8   dependency on delamination size and position by defining a lower bound on the propagation strain, through

9   bounding the delamination size, and finding the worst-case delamination depth within the laminate. This

10   updated method provides a conservative, rapidly computable figure of merit suitable for preliminary stacking

11   sequence optimisation, when exact delamination dimensions are unknown.

12   It should be noted that this paper does not provide a comprehensive method for damage tolerant laminate

13   design in a full statistical sense. Instead, analysis is limited to individual circular delaminations. This

14   approximation is not intended to mimic real damage morphology, which is much more complex, nor is it

15   intended to capture every failure mode. This method does, however, promote designs in which the outer layers

16   are selected to protect inner, more highly stressed layers, using a mechanics-based approach which captures

17   sufficient features of the opening of back face delaminations in the symmetric mode illustrated in Figure 1c). It

18   is emphasised that such a method does not constitute a safe methodology for certification, and in practice

19   resulting designs would require verification using high-fidelity modelling of more realistic damage

20   morphologies, and experimental testing at a damaged sub-component level.

21   *2.2. Delamination Propagation Strain*

22   Following [10], suppose a circular delamination with diameter ϕ and area A arises at a given ply interface

23   as shown in Figure 2. The choice of a circular delamination is an idealisation aimed at providing a conservative

24   bounding case when the exact delamination geometry is unknown. Delaminations are in practice much more

25   irregular, but are often idealised as elliptical, as in [10]. The orientation of the delamination relative to the

26   applied load will not be known a priori. A circular geometry is therefore taken as an outer boundary containing

27   all randomly-oriented elliptical delaminations with major dimension, ϕ. The delamination creates a sub-

28   laminate, which will buckle and blister under compressive strains, as shown in Figure 2b). A general two-

1   dimensional deformation state is assumed to exist with applied strain vector, $\boldsymbol{\varepsilon} = \left\{\varepsilon_x, \varepsilon_y, \gamma_{xy}\right\}^T$, with tensile

2   strains defined as positive. Identical strains are applied to both the laminate and sub-laminate to maintain

3   compatible strains at the laminate/sub-laminate boundary. The delamination is assumed to grow by area dA,

4   highlighted by the shaded regions in Figure 2.

5   The sub-laminate buckling strain is calculated using a thin-film assumption [5–7], such that the effects of

6   sub-laminate buckling upon buckling of the full laminate are neglected. The critical sub-laminate buckling strain

7   vector, $\boldsymbol{\varepsilon}_C$, is expressed as a factor of applied strain vector, as

8
$$\boldsymbol{\varepsilon}_C = F_C \boldsymbol{\varepsilon} \tag{1}$$

9   where F_C is the critical sub-laminate buckling factor. This factor must be determined numerically as no

10   closed-form solution exists for buckling of fully-coupled laminated plates with circular boundaries. In this

11   paper, finite strip program VICONOPT [11] is used for the sake of computational efficiency. The circular

12   delamination in Figure 2 is divided into a series of connected strips across its width, with compatibility and

13   equilibrium conditions satisfied along strip boundaries. VICONOPT uses the Wittrick-Williams algorithm [51]

14   to calculate the eigenvalues of the transcendental stiffness matrix derived from the exact solution of the

15   governing equations of the constituent strips, to give the buckling load factor of the minimum-energy mode.

16   Non-symmetric sub-laminates are allowed for in calculation of these eigenvalues, which are determined using a

17   fully populated ABD matrix. A clamped delamination boundary, with zero displacement in all degrees of

18   freedom, is modelled using VICONOPT point supports [52] at the intersection of each strip edge with the

19   delamination circumference. The continuous boundary is thereby discretised into point-wise constraints.

20   Periodic displacement functions are assumed which satisfy boundary conditions at these points. Point supports

21   are separated by 10-degree intervals around the circumference resulting in 18 strips and 36 supports, based upon

22   a previous convergence study [10].

23   Under further application of compressive strain, the delamination below the post-buckled sub-laminate will

24   propagate. This threshold propagation strain, $\boldsymbol{\varepsilon}_{th}$, is also expressed as a function of the applied strain, as

25
$$\boldsymbol{\varepsilon}_{th} = F_{th} \boldsymbol{\varepsilon} \tag{2}$$

26   It should be noted that an alternative threshold strain factor was employed in [10], which instead defined the

27   threshold strain as a factor of $\boldsymbol{\varepsilon}_C$, however, F_{th} is instead here expressed as a factor upon the applied strain, $\boldsymbol{\varepsilon}$,

1   for notational convenience. Assuming delamination growth is symmetric, as shown in Figure 2, a condition for

2   delamination growth was previously derived as [10]

3
$$G_C = (F_{th} - F_C)(F_{th} + 3F_C)\boldsymbol{\varepsilon}^T A_{SL} \boldsymbol{\varepsilon} \tag{3}$$

4   where A_{SL} is the sub-laminate in-plane stiffness matrix, and G_c is the critical Strain Energy Release Rate

5   (SERR) associated with delamination growth. Rearranging Eq. (3) yields the threshold strain factor as

6
$$F_{th} = F_C \left(\sqrt{4 + \frac{G_C}{F_C^2 \boldsymbol{\varepsilon}^T A_{SL} \boldsymbol{\varepsilon}}} - 1 \right) \tag{4}$$

7   *2.3. Threshold Strain Lower Bound*

8   The expression in Eq. (4) is dependent upon the delamination geometry via its dependency upon the sub-

9   laminate buckling factor F_C. It is, however, impossible to know the exact delamination dimensions during

10   design, as the damage has not occurred during this stage. A pragmatic, conservative bounding case is therefore

11   required for design purposes. An expression for the lowest possible strain factor $F_{th,min}$, independent of

12   delamination dimensions, may be obtained by minimising Eq. (4) with respect to F_C. By setting $\partial F_{th}/\partial F_C = 0$,

13   this minimum can be shown to be

14
$$F_{th,min} = \sqrt{\frac{3G_C}{4\boldsymbol{\varepsilon}^T A_{SL} \boldsymbol{\varepsilon}}} \tag{5}$$

15   This minimum can likewise be shown to arise at a buckling factor of

16
$$F_C = F_{th,min}/3 \tag{6}$$

17   This expression is independent of the delamination dimensions, however, remains dependent upon the

18   delamination depth via the sub-laminate in-plane stiffness matrix, A_{SL}, which has linear dependency upon sub-

19   laminate thickness. Eq. (5) is consequently inversely proportional to the sub-laminate thickness, and therefore

20   predicts lower threshold strains for delaminations further from the laminate surface. The actual threshold strain

21   factor, given by Eq. (4), tends asymptotically towards the sub-laminate buckling factor F_C with increasing A_{SL}.

22   As this buckling factor broadly increases with delamination depth, the lower bound provided by Eq. (5) is overly

23   conservative for some cases.

1   A less conservative worst-case threshold strain may be obtained by bounding the range of feasible

2 delamination sizes, by placing an upper bound on the assumed delamination diameter. Based upon previous

3 experimental observations of Barely Visible Impact Damage [9,53], the largest feasible delamination diameter,

4 ϕ_{max}, likely to arise from this damage is expected to be

5 $$\phi_{max} = 9t \tag{7}$$

6 where t is the laminate thickness. Note that it is unlikely that BVID will occur in particularly thick laminates. In

7 such cases a maximum damage size may instead be applied. Whilst the presented method relies upon the

8 damage size being bounded, the precise definition of this bound may be subject to engineering judgement. In

9 reality, damage can be characterised by multiple delaminations, typically increasing in size away from the

10 impact site. It is important that the upper bound, ϕ_{max}, encompasses the largest value in this range.

11 *2.4. Experimental Justification of Analytical Propagation Strain*

12   The two-dimensional propagation model outlined in Section 2, derived in [10], and subjected to a detailed

13 comparative study in [13] has previously been validated against experimentally-obtained propagation strains in a

14 range of laminates with artificial circular Polytetrafluoroethylene (PTFE) delaminations [10,13]. Readers are

15 referred to [8,10,13] for full details of these experimental results. Here, in order to justify the use of the plate

16 model for laminate optimisation considering Compression After Impact (CAI), the results of Eq. (4) are

17 compared with experimental failure strains obtained from CAI tests on laminates containing impact damage

18 [53].

19   In [53] laminates with three different quasi-isotropic stacking sequences were manufactured from AS4/8552

20 material, these are referred to as the: (i) Control laminate [45/0/-45/90]$_{4S}$, (ii) ±45° Outer laminate

21 [(±45)$_4$/(90/0)$_4$]$_S$, and (iii) 90° Outer laminate [90$_3$/45/90/-45$_3$/0/45$_3$/0$_2$/-45/0]$_S$.Lamina properties are taken as

22 $E_{11} = 128$ GPa, $E_{22} = 10.3$ GPa, $G_{12} = 6.0$ GPa, $v_{12} = 0.3$, with a ply thickness of 0.125mm [53]. All three

23 laminates were subject to 8J impacts whilst clamped over a 125×75mm ASTM D7136 window [54]. The extent

24 and depth of delamination damage was measured using an Ultrasonic Sciences C-scan system. From these data

25 it was possible to determine the maximum length of delaminations at the first eight interfaces ($i = 1, 2, 3, …8$)

26 from the back (non-impact) surface, as these interfaces contain the largest delaminations caused by the

27 impact. Axial compressive load was applied under displacement control, with each coupon restrained using a

1   circular anti-buckling guide centred on the damage region with an un-restrained window (on the back face) of

2   diameter 85mm. See [53] for details.

3   Analytical propagation strains are calculated for each of the three laminates described above by applying

4   Eq. (4) at each of the outer eight interfaces and obtaining the critical (minimum) value. Results of this analytical

5   study are compared against experimental propagation strains in Table 1. For each laminate, two damage

6   morphologies are modelled. Firstly, damage is modelled as a single circular delamination of diameter equal to

7   the maximum delamination dimension from the C-scan data at each interface. Each delamination is modelled in

8   isolation from the others, i.e. for each model run only a single delamination is assumed to exist. Secondly,

9   damage is modelled as a single circular delamination of diameter ϕ_{max}= 36mm, again in isolation, determined

10   using Eq. (7) with t = 4mm. Results from these two cases are shown in columns a) and b) of Table 1

11   respectively. Analytical propagation strains are determined for each assumed morphology for two limiting

12   cases of the Strain Energy Release Rate, specifically, $G_C = G_{IC}$ and $G_C = G_{IIC}$, as used in [13]. The

13   experimental propagation strains in Table 1 are taken from the strain data in Figure 6 of [53], which shows that

14   failure of the Control and 90° outer laminates occurred suddenly at the propagation strain. In the case of the

15   ±45° Outer laminate, stable propagation initiated at 5900 με, before failure at 7400 με, and as such, both values

16   are included in Table 1.

17   Where C-scan damage size data are used directly in the plate model (column a) of Table 1), the assumption

18   of pure Mode I or Mode II can be seen to provide reasonable lower and upper bounds upon the experimentally

19   observed strains. When the extent of damage is not known a priori, supplying constant diameter delaminations

20   given by Eq. (7) does not accurately predict the actual morphology, but does give a conservative lower bound

21   upon the experimental compression after impact results when $G_C = G_{IC}$ is assumed, (as shown in column b) of

22   Table 1). As such, throughout the remainder of this paper, Eq. (7) coupled with the assumption of $G_C = G_{IC}$ is

23   applied to produce a conservative figure of merit for CAI strength with low computational cost.

24   *2.5 Algorithm for Prediction of Threshold Strain Lower-bound*

25   An expression for the bounded minimum threshold propagation strain factor, $F_{th,lb}$, can be stated as

26   $$F_{th,lb} = \min \quad F_{th}(A_{SL,i}, \phi)$$

27   $$\text{subject to} \quad i \in 1, \dots, \lceil N/2 \rceil, \qquad 0 \leq \phi \leq \phi_{max} \tag{8}$$

where N is the number of plies, and $F_{th}\left(A_{SL,i}, \phi\right)$ is the strain factor for propagation of a delamination with diameter ϕ, located at the ith ply interface inducing a sub-laminate with in-plane stiffness A_{SL}, as given by Eq. (4). This expression searches across all ply interfaces and delamination sizes to find the lowest strain factor, arising at some critical depth. Rather than accurately modelling delamination size at each depth, which typically increases away from the impact site, it is assumed that the largest feasible delamination could arise at any depth. The purpose of Eq. (8) is to determine a conservative bounding case, rather than a realistic description of damage morphology. Noting that $\lceil\ \rceil$ denotes the ceiling operator which rounds up its argument to the nearest integer, Eq. (8) exploits symmetry by only searching over half of the laminate for the sake of computational efficiency. It is emphasised that the presented method is focused upon large, near back face delaminations, and in practice a minimum is typically found at 10-20% thickness.

An efficient method for finding this minimum is illustrated in Figure 3. As this method is to be applied in designing damage tolerance laminates, it is only instances in which the applied strain exceeds the delamination propagation strain (i.e. $F_{th,lb} < 1$) which are critical to guiding subsequent optimisation. A focus is therefore placed upon ascertaining if this is the case with the fewest possible sub-laminate buckling analyses to minimise the required computational expense, and a precise lower bound using Eq. (4) is only returned if $F_{th,lb} < 1$.

The outer loop (Figure 3a)) searches over delamination depth by assuming a delamination is located at each interface in turn starting from the laminate surface. At each interface the sub-laminate stacking sequence is updated, and a minimum strain factor within the range of feasible delamination diameters, $F_{th,i}$, is returned. If this factor is lower than those calculated from previous interfaces, the value of $F_{th,lb}$ is updated. The process is repeated until one of three stopping criteria is met:

- $F_C \geq 1.25$: The search has reached a depth at which sub-laminate buckling does not occur at the applied strain. A 25% margin is applied to prevent the through-thickness search stopping prematurely in instances in which the buckling factor reduces due to changes in the sub-laminate stacking sequence, thereby reducing the possibility of minima being missed by the search. Such situations may arise when, for instance, an additional 0° ply attracts more load to the sub-laminate.
- $F_{th,lb} \leq F_{th,i}$: The worst-case strain factor has been found and the critical depth passed, beyond which the factor typically increases.

1   • $i = \lceil N/2 \rceil$: The mid-plane has been reached. It should be noted that in practice this stopping criterion is

2   rarely active, with one of the other criteria terminating the search within 10-20% of the laminate depth.

3   Although optimisation in this paper is limited to symmetric stacking sequences, the method could be

4   applied to non-symmetric stacking sequences by searching over the entire stack, replacing $\lceil N/2 \rceil$ with

5   N in Eq. (8). In such applications the search should start from the ply on the back face of the laminate.

6 At each interface, an efficient subroutine is used to find the minimum strain factor, $F_{th,i}$. (Figure 3b)).

7 Unbounded minimum $F_{th,min}$ is first calculated using Eq. (5) assuming $G_C = G_{IC}$. If $F_{th,min} \geq 1$, sub-laminate

8 buckling analysis is unnecessary, as the applied strain does not exceed the lowest possible threshold strain at this

9 interface. Otherwise, it is necessary to determine whether this minimum corresponds to a delamination with

10 diameter within the feasible range. This check is performed by comparing the outputs of a single VICONOPT

11 buckling analysis, assuming the largest feasible delamination diameter ϕ_{max}, against the minimum given in

12 Eqs. (5-6). Two possible outcomes are illustrated in Figure 4. Noting that F_C is inversely proportional to ϕ^2, a

13 fixed point on the horizontal axis of Figure 4 corresponds to a fixed delamination diameter, and all points to the

14 right to smaller diameter delaminations. If the F_C calculated assuming diameter ϕ_{max} is lower than $F_{th,min}/3$,

15 (example a)), the unbounded minimum $F_{th,min}$ must belong to a delamination within the feasible range. This

16 value is consequently retained as $F_{th,i}$. If the calculated F_C is higher than $F_{th,min}/3$, (example b)), a

17 delamination with diameter ϕ_{max} has the lowest threshold strain in the feasible range. In this case, $F_{th,i}$ is

18 updated by applying Eq. (4) to the corresponding F_C.

19 An illustrative example of strain factor trends with respect to delamination depth is shown in Figure 5,

20 assuming an applied strain of $\boldsymbol{\varepsilon} = \{-4500, 3500, 0\}^T \mu\varepsilon$, and sub-laminates taken from sequence

21 $[45/-45_2/0_2/90/\pm45/\dots]$, arising on the back face of some larger stack. Each ply is divided into smaller intervals

22 to illustrate notional continuous variations in delamination depth. Trends are illustrated for unbounded minimum

23 $F_{th,min}$, and sub-laminate buckling and threshold propagation factors for a delamination with diameter $\phi_{max} =$

24   50mm.

25 Unbounded minimum threshold strain factor, $F_{th,min}$, decreases monotonically with delamination depth.

26 The threshold strain factor associated with the maximum delamination size, $F_{th}(\phi_{max})$, follows a similar

27 decreasing trend up to a depth of 0.625mm where these plots coincide, after which $F_{th}(\phi_{max})$ more closely

28 follows the trend of the underlying buckling factor, $F_C(\phi_{max})$. Strain factor lower bound, $F_{th,i}$, is given by

1 $F_{th,min}$ for delamination depths lower than 0.625mm, and $F_{th}(\phi_{max})$ otherwise. This strain factor falls below

2 unity at the fourth interface to a value of 0.94, indicating that the applied strain exceeds the threshold strain. The

3 algorithm in Figure 3 determines this factor by iterating through each ply interface from the outer surface. As

4 $F_{th,min} > 1$ for the first three interfaces, no buckling analysis is undertaken until the fourth interface. Here, a

5 single sub-laminate buckling analysis is used to determine $F_C(\phi_{max})$ and its corresponding $F_{th}(\phi_{max})$, and

6 ascertain: i) if this lies to the right of the minimum in Figure 4 and may therefore be used as the lower bound,

7 and ii) if this less conservative lower bound is also lower than one. An additional buckling analysis is

8 undertaken at the fifth interface to verify that the threshold strain factor increases for delaminations at greater

9 depths. This additional analysis indicates that the threshold strain factor increases to 0.95 at the fifth interface,

10 and as such the lower value of 0.94 calculated at the fourth interface is taken as critical. In this instance, two

11 buckling analyses are required to search the entire laminate depth and feasible range of delamination diameters.

12 ## 3. COMPATIBILITY INDEX FOR LAMINATE FORMABILITY

13 The tendency for wrinkles to arise during high-rate forming has been shown to depend upon the stacking

14 sequence of the flat preform [19–21]. In previous work [27], a Compatibility Index was proposed for rapid

15 prediction of the tendency of such defects to arise in different stacks. This index is based upon the concept that

16 facilitating compatible, low-energy deformation modes across multiple plies, prevents wrinkles from occurring.

17 Each ply is assumed able to deform in one of three in-plane deformation modes, given by the eigenvectors

18 of the lamina stiffness matrix of a rotated, uncured ply, Q^*. This matrix is expressed in Kelvin notation [55,56]

19 to ensure stress and strain share the same basis. Using this notation, the constitutive relationship of a rotated ply

20 is stated as

21
$$\boldsymbol{\sigma} = \begin{pmatrix} \sigma_{11} \\ \sigma_{22} \\ \sqrt{2}\sigma_{12} \end{pmatrix} = \begin{bmatrix} Q_{11}^* & Q_{12}^* & \sqrt{2}Q_{16}^* \\ Q_{12}^* & Q_{22}^* & \sqrt{2}Q_{26}^* \\ \sqrt{2}Q_{16}^* & \sqrt{2}Q_{26}^* & 2Q_{66}^* \end{bmatrix} \begin{pmatrix} \varepsilon_{11} \\ \varepsilon_{22} \\ \sqrt{2}\varepsilon_{12} \end{pmatrix} = Q^* \boldsymbol{\varepsilon} \tag{9}$$

22 where ply stiffnesses Q_{ij}^* are expressed in the Voight notation commonly used in Classical Lamination Theory

23 [35], and ε_{12} denotes tensor shear strain. Example eigenvectors of the Q^* matrix of a 0° ply are illustrated in

24 Figure 6, where $\boldsymbol{v}_i$ denotes the ith eigenvector. It should be noted that the exact eigenvectors for modes 1 and 3

contain very small Poisson deformations, however, these are often negligible if the resin-dominated transverse

modulus E_{22} is small relative to fibre direction modulus E_{11}.

The scalar product of the eigenvectors of two adjacent plies may be used as a measure of the compatibility

of the potential resin-dominated deformation modes in these plies, defined as

$$c_{i,j}(\theta_1, \theta_2) = \boldsymbol{v}_i(\theta_1)^T \boldsymbol{v}_j(\theta_2) \tag{10}$$

where subscripts i and j refer to resin-dominated deformation modes, and 1 and 2 to ply indices. A

compatibility of 1 indicates that two modes are identical, whereas 0 indicates complete incompatibility.

Laminate compatibility may be defined by assuming that a stack with a large number of adjacent plies with

high compatibility between modes 1 or 2 will be more formable. In such stacks, deformation is facilitated in

large zones of plies with compatible modes, and slip-planes arise between these zones. Stacks with poor

formability have many adjacent plies with low compatibility between resin modes, causing high-energy fibre

modes to restrict deformation and wrinkles to arise. A sign convention is prescribed upon positive shear

(Mode 2) to preserve the right-handed sign convention of a rotated 0° ply. It is also necessary to account for

shear in the opposite direction, which is henceforth referred to as Mode 2*, with eigenvector given by

$\boldsymbol{v}_{2^*} = -\boldsymbol{v}_2$ as depicted in Figure 6. It is assumed that a stack will tend to deform via the combination of ply

modes which result in the highest possible laminate compatibility. This maximum compatibility, C_{max}, is

defined as [27]

$$C_{max} = \max_{i_1,...,i_N} \frac{1}{(N-1)} \sum_{j=1}^{N-1} c_{i_j,i_{j+1}}(\theta_j, \theta_{j+1}) \text{ where } \mathrm{i}_j \in \{1,2,2^*\} \, \forall \, j = 1,...,N-1 \tag{11}$$

where $c_{i_j,i_{j+1}}(\theta_j, \theta_{j+1})$ is the compatibility of modes with index prescribed by i_j and i_{j+1} in the jth and $(j+1)$th

ply respectively, as calculated using Eq. (10), and N is the number of plies. Eq. (11) is an optimisation problem

for finding the set of indices, $i_1,...,i_N$, which give the highest laminate compatibility from a potential 3^N

combinations. An enumeration method was previously employed [27], wherein the maximum compatibility was

found by calculating compatibility for every possible mode combination. This method is impractical for stacks

with a large number of plies, rendering it unsuitable for use within optimisation. A more efficient method for

calculating C_{max} may be achieved by re-expression as a linear integer programming problem, stated as

14

$$C_{max} = \max_{x} \boldsymbol{f}^T \boldsymbol{x} = \frac{1}{(N-1)} \sum_{i=1}^{N-1} \sum_{j,k \in \{1,2,2^*\}} c_{j,k}(\theta_i, \theta_{i+1}) x_{ijk}, \text{ where } x_{ijk} \in \{0,1\} \tag{12}$$

Instead of summing over plies, this revised formulation sums over ply interfaces via index i. One of nine possible compatibility values, $c_{j,k}(\theta_i, \theta_{i+1})$, is allocated to each interface using binary variables x_{ijk}. Indices j and k allocate one of three deformation modes to plies either side of the interface, yielding these nine possible values. For instance, if $x_{122^*} = 1$, ply 1 is taken to deform in mode 2 and ply 2 this taken to deform in mode 2^*, contributing $c_{2,2^*}(\theta_1, \theta_2)$, to the sum in Eq. (12). The maximum possible stack compatibility is determined by finding the set of $9(N-1)$ x_{ijk} values which maximise the overall sum.

Exactly one compatibility value must be assigned to every interface. This condition is enforced by optimising Eq. (12) subject to a set of $N-1$ equality constraints, which are defined as

$$\sum_{j,k \in \{1,2,2^*\}} x_{ijk} = 1 \ \forall \ i \in 1, \dots, N-1 \tag{13}$$

Because deformation modes are assigned to interfaces rather than plies, it is also necessary to ensure that no individual ply is assumed to deform in more than one mode within a given sum. For instance, x_{122^*} and x_{211} cannot simultaneously equal 1, as this would require ply 2 to simultaneously deform in Modes 2^* and 1. These conditions are enforced via a set of $54(N-2)$ inequality constraints, which are defined as

$$x_{ijk} + x_{(i+1)lm} \leq 1 \ \forall \ i \in \{1, \dots, N-2\}, \quad j,k,l,m \in \{1,2,2^*\} \text{ with } k \neq l \tag{14}$$

In this paper, Eqs. (12-14) are solved using MATLAB [57] linear integer programming solver '*intlinprog*', which uses a branch-and-bound method. This implementation enables calculation of the compatibility index for a 100-ply stack in less than 1 second on a standard desktop computer.

This compatibility index has been validated by forming a number of flat 24-ply stacks with differing stacking sequence over a male tool featuring regions of double curvature using a Double Diaphragm Former. [27]. The tool geometry was that of a C-spar with a central recessed, 'joggle' region, bounded by 1:20 ramps in both the flanges and web (see for [27] details). Flat rectangular laminates were initially manufactured from AS4/8552 UD prepreg. These laminates were sandwiched between two layers of vacuum bagging material, supported above the forming tool, which was placed upon the bed of the former. Following a full debulking cycle, the stacks were heated to a temperature of 60°C, and a vacuum applied from the forming bed at a rate of

1   0.7 bar/minute until full vacuum was reached. The vacuum bags were consequently drawn into the cavity

2   between the tooling and forming bed, causing the laminate to conform to the tool geometry. The formed spars

3   were subsequently cured in an autoclave following the manufacturer's recommended curing cycle.

4   Three of the C-spars manufactured using the described process are illustrated in Figure 7, which shows the

5   outer (non-tool) surface of the web of these spars; the region in which wrinkling, when it occurred, was most

6   severe. Stacks with low C_{max}, in the range, 0.5-0.65, such as the example in Figure 7c), were found to be

7   severely wrinkled. Stacks with higher compatibility values, with $C_{max} \geq 0.85$, such as the example in Figure

8   7a), resulted in wrinkle-free parts. Stacks with intermediate C_{max} values, such as the example in Figure 7b),

9   exhibited an intermediate level of wrinkling. The interested reader is referred to [27] for further details of both

10 these experimental trials and the underlying theoretical framework, including results for other stacking

11 sequences.

12 ## 4. OPTIMISATION FRAMEWORK

13 ### *4.1. Stage I: Lamination Parameter Optimisation*

14 #### 4.1.1. Overview

15   The first stage of the optimisation procedure is to tailor homogenised component stiffnesses by optimising

16 lamination parameters, in order to minimise structural mass subject to constraints which ensure structures

17 perform within prescribed limits under loading. This optimisation problem is defined as:

18 $$\min M(\boldsymbol{x}) \tag{15}$$

19 Subject to

20 $$g_i(\boldsymbol{x}) \leq 0 \qquad i = 1, \dots, n_g \tag{16}$$

21 $$\underline{x_j} \leq x_j \leq \overline{x_j} \quad j = 1, \dots, d \tag{17}$$

22   where $M(\boldsymbol{x})$ is the overall mass, $\boldsymbol{x} = \{x_1, \dots, x_d\}$ is a vector of d design variables constrained between

23 lower and upper bounds $\underline{x_j}$ and $\overline{x_j}$ respectively, and each $g_i(\boldsymbol{x})$ is one of n_g constraints to which the optimisation

24 is subjected. Details of each of these terms are outlined in the sections below, with design variables defined in

25 Section 4.1.2, and constraints in Sections 4.1.3-4.1.4. Throughout, it is assumed that laminates are symmetric

such that there is no in-plane and out-of-plane coupling, and plies are restricted to standard orientations of 0°,

90°, 45° and -45°. These assumptions are made for consistency with current industrial practices, to demonstrate

applicability of the new formability and damage tolerance constraints alongside such design requirements. It

should be noted that the use of symmetric stacking sequences is not a necessary condition for eliminating

membrane-bending coupling, and there is no manufacturing-based reason for restricting ply orientations to this

set of standard angles. These assumptions therefore restrict the set of feasible stacking sequences to a smaller set

than is strictly necessary for achieving the desired behaviour. Improved designs may be achieved by relaxing

these constraints on stacking sequence.

4.1.2. Design Variables

In-plane and out-of-plane lamination parameters may be defined as [35]

$$\xi^A_{[1,2,3,4]} = \frac{1}{2}\int_{-1}^{1}[\cos 2\theta\,(\bar{z}),\cos 4\theta\,(\bar{z}),\sin 2\theta(\bar{z}),\sin 4\theta(\bar{z})]d\bar{z} \tag{18}$$

$$\xi^D_{[1,2,3,4]} = \frac{3}{2}\int_{-1}^{1}[\cos 2\theta\,(\bar{z}),\cos 4\theta\,(\bar{z}),\sin 2\theta(\bar{z}),\sin 4\theta(\bar{z})]\bar{z}^2 d\bar{z} \tag{19}$$

where $\xi^A_{[1,2,3,4]}$ and $\xi^D_{[1,2,3,4]}$ denote the in-plane and out-of-plane lamination parameters respectively, $\bar{z}$ is the

normalised through-laminate thickness coordinate $\bar{z} = \frac{2z}{t}$, and $\theta(\bar{z})$ is the layup function which denotes

variations in ply orientation over the thickness. Lamination parameters are related to laminate stiffnesses by the

expressions

$$\begin{pmatrix} A_{11} \\ A_{22} \\ A_{12} \\ A_{66} \\ A_{16} \\ A_{26} \end{pmatrix} = t \begin{bmatrix} 1 & \xi^A_1 & \xi^A_2 & 0 & 0 \\ 1 & -\xi^A_1 & \xi^A_2 & 0 & 0 \\ 0 & 0 & -\xi^A_2 & 1 & 0 \\ 0 & 0 & -\xi^A_2 & 0 & 1 \\ 0 & \xi^A_3/2 & \xi^A_4 & 0 & 0 \\ 0 & \xi^A_3/2 & -\xi^A_4 & 0 & 0 \end{bmatrix} \begin{pmatrix} U_1 \\ U_2 \\ U_3 \\ U_4 \\ U_5 \end{pmatrix} \tag{20}$$

$$\begin{pmatrix} D_{11} \\ D_{22} \\ D_{12} \\ D_{66} \\ D_{16} \\ D_{26} \end{pmatrix} = \frac{t^3}{12} \begin{bmatrix} 1 & \xi^D_1 & \xi^D_2 & 0 & 0 \\ 1 & -\xi^D_1 & \xi^D_2 & 0 & 0 \\ 0 & 0 & -\xi^D_2 & 1 & 0 \\ 0 & 0 & -\xi^D_2 & 0 & 1 \\ 0 & \xi^D_3/2 & \xi^D_4 & 0 & 0 \\ 0 & \xi^D_3/2 & -\xi^D_4 & 0 & 0 \end{bmatrix} \begin{pmatrix} U_1 \\ U_2 \\ U_3 \\ U_4 \\ U_5 \end{pmatrix} \tag{21}$$

where t is the laminate thickness and U_{1-5} are material invariants [35]. Suppose a structure is partitioned

into multiple regions, the properties of which are to be optimised independently. These properties are optimised

by varying each of the in-plane and out-of-plane lamination parameters, and the laminate thickness. Due to the

restriction of plies to standard orientations of 0°, 90°, 45° and -45°, $\xi_4^{A,D}$ are automatically zero [58] and, as

such, are not varied in the optimisation. Additionally, extension-shear and bend-twist coupling parameters, $\xi_3^{A,D}$,

are constrained to zero, resulting in five design variables per region. Lamination parameters are bounded within

the interval [-1, 1] in the general case, whereas thicknesses may adopt any positive, real value. In practice,

problem-specific bounds are placed upon the thickness to improve convergence. Given these pre-defined

bounds, all design variables are non-dimensionalised through transformation onto the unit interval, [0, 1], to

further improve performance.

4.1.3. Lamination Parameters Feasibility Constraints

Lamination parameters are not independent and must be bounded within feasible regions defined by

inequality constraints, which describe the convex hull of feasible lamination parameter values. A full set of

expressions for these feasible regions, given the assumed restrictions on ply angle, were derived in [58].

Following substitution of $\xi_3^{A,D} = 0$ into these expressions, and elimination of non-active constraints, the feasible

region may be using:

$$2\left|\xi_1^{A,D}\right| - \xi_2^{A,D} - 1 \leq 0 \tag{22}$$

$$\frac{1}{4}(\xi_i^A + 1)^3 - 1 \leq \xi_i^D \leq \frac{1}{4}(\xi_i^A - 1)^3 + 1 \quad i = 1,2 \tag{23}$$

$$(2\xi_1^A - \xi_2^A - 1)^4 - 16(2\xi_1^D - \xi_2^D - 1)(2\xi_1^A - \xi_2^A - 1) \leq 0 \tag{24}$$

$$(2\xi_1^A + \xi_2^A + 1)^4 - 16(2\xi_1^D + \xi_2^D + 1)(2\xi_1^A + \xi_2^A + 1) \leq 0 \tag{25}$$

$$(2\xi_1^A - \xi_2^A + 3)^4 - 16(2\xi_1^D - \xi_2^D + 3)(2\xi_1^A - \xi_1^A + 3) \leq 0 \tag{26}$$

$$(2\xi_1^A + \xi_2^A - 3)^4 - 16(2\xi_1^D + \xi_2^D - 3)(2\xi_1^A + \xi_2^A - 3) \leq 0 \tag{27}$$

In line with current industrial practices, lamination parameters are further constrained to ensure at least 10%

of plies are taken from each permissible orientation. Lamination parameter feasible regions are reduced in size

by assuming a maximum proportion of 70% of plies in each orientation. Resulting vertices of the outer

boundary of these regions are given by three points in the ξ_1^A-ξ_2^A plane [59], and six points in the ξ_1^D-ξ_2^D plane [60], as illustrated in [61]. The interested reader is referred to [59] for a detailed discussion on these outer boundaries. These constraints are enforced by updating the bounds on the lamination parameters to $-0.6 \leq \xi_{1,2}^A \leq 0.6$, $-0.972 \leq \xi_1^D \leq 0.972$, and $-0.984 \leq \xi_2^D \leq 0.984$, using the method described in [61]. When lamination parameters are transformed onto the unit interval using these updated bounds, as described in Section 4.1.2, the feasible region expressions in Eqs. (22-27) are automatically scaled to enforce the 10% rule. For example, substituting the updated bounds on Eq. (22) into $\xi_{1,2}^A$ leads to

$$2|\xi_1^A| - \xi_2^A - 0.6 \leq 0 \tag{28}$$

$$\xi_2^A - 0.6 \leq 0 \tag{29}$$

Note that this method results in approximating the outer boundary on the ξ_1^D-ξ_2^D plane as triangular.

4.1.4. Structural Constraints

Buckling constraints are applied to ensure structures do not buckle under applied loads, stated as

$$\frac{1}{F_i} - 1 \leq 0 \tag{30}$$

where F_i is the eigenvalue corresponding to the ith buckling mode. Each eigenvalue represents the reserve factor of the critical vector of stress resultants, $\boldsymbol{N}_{C,i}$, relative to applied resultants, $\boldsymbol{N}$, via the relationship

$$\boldsymbol{N}_{C,i} = F_i \boldsymbol{N} \tag{31}$$

These eigenvalues may be determined using an eigenvalue buckling solver, and are here calculated using finite element analysis. Strain constraints are applied to ensure the magnitude of components of the strain vector do not exceed a target value, $\varepsilon_{t,i}$, known in the aerospace industry as a strain allowable, stated as

$$\frac{\max\{|\varepsilon_i|\}}{\varepsilon_{t,i}} - 1 \leq 0 \tag{32}$$

where ε_i is a component of the strain vector, with $i = x, y, xy$. A maximum absolute value is taken across all elements of the finite element model. This constraint ensures strains are within the correct vicinity such that damage tolerant designs are achievable during the second stage of the optimisation.

19

4.1.5. Sensitivity Analysis

An accurate measure of the partial derivatives of objectives and constraints with respect to the design variables is required for use of gradient-based solvers. It is trivial to obtain closed-form solutions for the sensitivities of the mass, and lamination parameter feasibility constraints. Sensitivities of the strain and buckling constraints are approximated using forward finite differences by applying a small perturbation, Δx, to each non-dimensionalised design variable, and calculating the resulting rate of change. After a convergence study, a value of $\Delta x = 10^{-4}$ was used.

As finite element software outputs buckling factors in ascending order rather than by mode, it is important to ensure that each perturbed buckling factor is paired to the unperturbed factor with the same mode shape. Here, each factor is paired with that which yields the highest Modal Assurance Criterion (MAC) value, given as

$$\text{MAC} = \frac{\left(\boldsymbol{\varphi}_i^T \boldsymbol{\varphi}_j\right)^2}{\left(\boldsymbol{\varphi}_i^T \boldsymbol{\varphi}_i\right)\left(\boldsymbol{\varphi}_j^T \boldsymbol{\varphi}_j\right)} \tag{33}$$

where $\boldsymbol{\varphi}_i$ is the eigenvector of the ith buckling mode, and a MAC of 1 indicates identical eigenvectors and 0 completely dissimilar eigenvectors. A similar sorting algorithm was applied in [62].

4.2. Stage II: Stacking Sequence Optimisation

The aim of the second stage of the optimisation is to find a practical stacking sequence which closely matches the optimum lamination parameters values determined in Stage I, while conforming to industrial design rules and achieving the desired laminate formability and damage tolerance. The new formability and damage tolerance constraints are applied during this stage as they primarily depend upon stacking sequence rather than homogenised laminate-level properties. These constraints are relatively inexpensive to compute, and therefore suitable for optimisation using genetic algorithms, which typically require a large number of model evaluations.

The optimum lamination parameters are targeted by minimising the square difference between the target parameters, and those corresponding to a candidate stacking sequence, expressed as

$$\min_{\theta_1,\dots,\theta_{\left\lceil\frac{N}{2}\right\rceil}} P\left(\sum_{i=1}^{3}\left(\xi_i^A(\theta_1,\dots,\theta_N) - \xi_{i,opt}^A\right)^2 + \sum_{i=1}^{2}\left(\xi_i^D(\theta_1,\dots,\theta_N) - \xi_{i,opt}^D\right)^2\right) \tag{34}$$

where design variables $\theta_1,\dots,\theta_{\left\lceil\frac{N}{2}\right\rceil}$ denote a candidate stacking sequence with lamination parameters ξ_{1-3}^A ξ_{1-2}^D, and $\xi_{i,opt}^{A,D}$ are the optimum lamination parameters from Stage I, and P is a multiplicative penalty function

used to enforce constraints. Symmetry is automatically enforced by only optimising half of the plies, rounded to the nearest integer when the total number of plies is odd. Balanced stacking sequences are not explicitly enforced. Instead, a target value of $\xi_{3,opt}^A = 0$ is used such extension-shear coupling is minimised, permitting a small amount of imbalance should this enable a better match for the other lamination parameters. Each ply orientation may take permissible values from the set $\{-45°, 0°, 45°, 90°\}$, encoded as integers $\{1,2,3,4\}$ respectively. Each of the $\lceil N/2 \rceil$ design varibles may take one of these four integer values. An additional constraint ensures that no more than four plies of the same orientation are stacked contiguously following the method of [63], the penalty value used enforce this constraint is expressed as

$$P_{cont} = \sum_{i=1}^{4} \Theta_i \tag{35}$$

The value of Θ_i is 1 if four or more plies of the ith permissible orientation are stacked contiguously anywhere in the laminate and is zero otherwise. Due to the assumed restrictions upon ply orientation, there are four Θ_i terms.

To ensure that the condition that 10% of plies must belong to each of the permissible orientations, initially enforced during Stage I as described in Section 4.1.3, is not subsequently violated in Stage II, this constraint is reapplied using a penalty term defined as

$$P_{10\%} = \sum_{i=1}^{4} \Pi_i, \quad \text{where } \Pi_i = \begin{cases} 0.1N - N_{\theta_i} & \text{when } N_{\theta_i} < 0.1N \\ 0 & \text{otherwise} \end{cases} \tag{36}$$

where N_{θ_i} is the total number of plies with orientation θ_i, and there are total of four penalty terms, Π_i, each corresponding to one of the permissible orientations.

A formability constraint is applied, defined as

$$C_{max} \geq 0.85 \tag{37}$$

where C_{max} is the compatibility index, as defined in Section 3. A target compatibility of 0.85 is chosen, as this value was found to be a lower bound for stacks less prone to wrinkling during forming in previous Double Diaphragm Forming trials [27]. This formability constraint is applied via a penalty term, defined as

$$P_{C_{max}} = \begin{cases} (0.85 - C_{max})/0.85 & \text{when } C_{max} < 0.85 \\ 0 & \text{otherwise} \end{cases} \tag{38}$$

The damage tolerance constraint is expressed as

$$F_{th,lb} \geq 1 \tag{39}$$

where $F_{th,lb}$ is the lower bound on the factor of the applied strain at which a delamination arising from BVID would be expected to propagate, calculated using Eq. (8). $F_{th,lb}$ is defined as a factor of an applied strain vector, $\boldsymbol{\varepsilon}$, which is required as input to the algorithm in Figure 3. This strain vector is taken directly from the finite element model output, assuming the optimum parameters arising from Stage I. Note that this assumption introduces a discrepancy between the strain vector used in the damage tolerance model, and that achieved by a given candidate stacking sequence. Depending upon the distance between the target lamination parameters and those of a given design, this discrepancy could be large, although it will be smaller for designs with lamination parameters closer to the target. The damage tolerance constraint is applied using a penalty term, expressed as

$$P_{DT} = \begin{cases} 1 - F_{th,lb} & \text{when } F_{th,lb} < 1 \\ 0 & \text{otherwise} \end{cases} \tag{40}$$

A memory capability is embedded into the genetic algorithm to improve efficiency, such that threshold strain factors are stored each time a new sub-laminate combination is encountered. These factors are looked up whenever this sub-laminate recurs during the optimisation process. The overall number of sub-laminate buckling calculations is thereby reduced, exploiting the fact that a given sub-laminate may belong to a much larger number of potential overall stacking sequences.

The overall penalty term, P, in Eq. (34), is calculated by compiling the penalty terms associated with the stacking sequence, formability and damage tolerance constraints, as

$$P = (1 + P_{10\%} + P_{cont})^p \left(1 + P_{C_{max}}\right)^q (1 + P_{DT})^r, \tag{41}$$

where exponents p, q and r govern the strength with which the different penalties are applied.

Note that this well-established [40,42], two-stage method does not guarantee an exact match between the target lamination parameters and those achieved by the optimised stacking sequence. Such a match is unlikely to exist given a fixed number of plies, the imposed restrictions upon ply orientation and stacking sequence, and other practical design constraints. It is considered pragmatic to instead aim to find as close a match as is possible, given the range of competing design requirements often imposed in industry.

5. NUMERICAL EXAMPLES

5.1. Overview

The proposed framework is demonstrated upon two example optimisation problems, namely, a flat plate and a blade-stiffened wing panel, both modelled in finite element software ABAQUS [64]. Cured material properties of Hexcel T700GC/M21 prepreg are assumed as $E_{11} = 136$ GPa, $E_{22} = 8.9$ GPa, $G_{12} = 4.5$ GPa, $v_{12} = 0.35$, $G_{IC} = 550$ J/m^2, and a ply thickness of 0.25mm. The damage tolerance model has previously been validated against experiments using this material [10]. Eigenvectors used in the formability constraint are taken directly from [27]. Stage I of the optimisation is undertaken using the MATLAB gradient-based solver '*fmincon*' [57] using the interior-point method, and stage II using the MATLAB genetic algorithm function '*ga*' [57]. Design variables are restricted to the integer values outlined in Section 4.2 using integer constraints. A population size of 20, with 2 elite children retained at each generation, and crossover probability of 0.8, , are used alongside stochastic uniform selection, Laplace crossover, and power mutation functions, as are recommended when using integer constraints [65]. The genetic algorithm is run for 100 generations. Exponents of the penalty terms in Eq. (41) were set to values of: $p = 1$, $q = 2$, and $r = 2$. The above parameters for tuning the genetic algorithm were selected based upon a trial-and-error experience, with the aim of achieving a consistently good match to target lamination parameters within a reasonable number of model evaluations. It is noted that a larger population size or number of generations may achieve better results, at the expense of more model evaluations. Genetic algorithms are stochastic in nature, and therefore are not guaranteed to return the same solution when repeatedly applied to the same problem. In the following examples, the genetic algorithm is evaluated five times and results are presented for the best run. The collective outcomes of both examples are discussed in Section 6.

5.2. Flat Plate

The first numerical example is a flat plate of length, a, and width, b, under design compressive load P_x applied as uniform end-shortening, as shown in Figure 8. Plate dimensions, loading and boundary conditions are taken from [66]. Longitudinal edges are assumed to be stress-free, with all edges modelled as simply-supported in the z direction. The plate is modelled using 4800 S4R quadrilateral shell elements, based upon convergence of the first five buckling modes to three significant figures, while ensuring a minimum of five nodes per half-

| 1 | wavelength for each mode shape [42]. Laminate properties are inputted as "General Shell Stiffnesses" (see |

<table>
<tr><td>1</td><td>wavelength for each mode shape [42]. Laminate properties are inputted as "General Shell Stiffnesses" (see</td></tr>
</table>

1   wavelength for each mode shape [42]. Laminate properties are inputted as "General Shell Stiffnesses" (see

2   Section 29.6.6 of [67]), to enable their definition using lamination parameters. Using this method, laminate A

3   and D matrices, as calculated using Eqs. (20-21), may be inputted directly to Abaqus. Transverse shear

4   stiffnesses were taken as their default values for a general shell section, an approximation defined using in-plane

5   stiffnesses A_{11}, A_{22} as well as A_{66}, as defined in Section 29.6.4 of [67]. Whilst it is emphasised that these values

6   do not accurately account for the resin-dominated through-thickness shear deformation, and will result in a

7   small over-prediction of buckling loads, such a compromise was considered acceptable for this exercise in

8   demonstrating the new formability and damage tolerance constraints. Minimum-mass optimisation is achieved

9   by minimising the plate thickness.

10   While a plate does not itself constitute a challenging forming problem, the purpose of this example is to

11   generate a range of target stiffnesses over which to demonstrate the applicability of the damage tolerance and

12   formability constraints. These stiffnesses are generated in a parametric study, in which the strain allowable in

13   Eq. (32) is varied between 1000με and 6000με to alter the relative importance of strain and buckling to design.

14   The stacking sequences resulting from each optimisation run are shown in Table 2. The corresponding

15   lamination parameters and thicknesses are shown in Table 3, which details the optimum parameters from Stage I

16   alongside the approximate match achieved in the discrete stacking sequence optimisation of Stage II. Note that

17    $\xi_4^{A,D} = 0$ after both Stages I and II in all examples, as this condition is automatically met by restricting plies to

18   orientations of 0°, 90°, 45° and -45°, and as such, these values are omitted from Table 3. Values of laminate

19   buckling and strain constraints from both optimisation stages are shown in Table 4 alongside parameters relating

20   to damage tolerance and formability. For damage tolerance, the lower bound on delamination propagation strain

21   and the corresponding reserve factors are shown, with $F_{th,lb}$ expressed as a factor of the longitudinal strain

22   arising from Stage II. The total number of sub-laminate buckling analyses required throughout the optimisation,

23   N_{runs}, are shown in order to demonstrate the efficiency of the method. Additionally, ply interface level plots of

24   the lower bound on delamination propagation strain are shown in Figure 9. Formability is indicated by C_{max}.

25   Designs driven by lower target strains are pushed towards $\xi_{1,2}^A = 0.6$, corresponding to the maximum

26   proportion of 0° plies permitted by the 10% rule. The 1000 με strain allowable is so stringent that the buckling

27   constraint is not active in this example. Designs with higher target strains are buckling driven and are pushed

28   towards $\xi_1^D = 0$, $\xi_2^D = -0.98$, corresponding to the maximum proportion of ±45° plies permitted by the 10% rule.

The 6000 με example is entirely buckling driven as the strain constraint is no longer active. All intermediate

designs form a line between these two points, with in-plane parameters limited by the strain constraint, and out-

of-plane parameters by buckling. This parametric study thereby provides a variety of target lamination

parameters against which to test the damage tolerance and formability constraints, the outcomes of which are

discussed in Section 6.

The lamination parameters achieved in Stage II of the optimisation agree with their target values to

differing extents. The best agreement across all parameters is achieved by stack a), which may be due to the

large number of plies in this laminate giving rise to a larger number of feasible stacking sequences and therefore

greater flexibility. A good agreement is achieved in the out-of-plane lamination parameters $\xi_{1,2}^D$ for all examples.

Larger discrepancies can, however, be noted in ξ_1^A of stack b), and in ξ_2^A of stacks d) and e). In each case, Stage

II of the optimisation was limited by the 10% rule. For stacks d) and e), given a total of 26 plies, there must be a

minimum of four plies of each of 0, 90, 45, and -45° to satisfy both the 10% and symmetry constraints. The

value of ξ_2^A= -0.385 corresponds to stacks with the maximum feasible number of 45° and -45° plies, and is the

closest achievable value to the Stage I target of ξ_2^A= -0.6. Similarly, the value of ξ_1^A = 0.429 in stack b)

corresponds to the maximum feasible number of 0° plies in a symmetric 28-ply laminate.

Examples a), b) and c) all meet the target of $\xi_3^A = 0$, thereby eliminating extension-shear coupling as

desired. Conversely, examples d) and e) have small, non-zero values of ξ_3^A. In these cases it is impossible to

generate a symmetric 26-ply stack which is sufficiently 45-dominated to meet the target values of $\xi_{1,2}^A$, while

being both balanced and satisfying the 10% rule, and so the optimisation prioritises the latter criterion. Noting

by inspection that example c) satisfies both the buckling and strain constraints for both examples d) and e), and

is the same thickness, this layup better meets all design criteria. Bend-twist coupling parameter ξ_3^D is low, but

non-zero in each example, with the largest discrepancy corresponding to a value of ξ_3^D = -0.125 in stack b). Such

an outcome is common, as bend-twist coupling is strongly dependent on the ordering of plies and, as such, is

more difficult to eliminate than extension-shear coupling (if symmetry is enforced). It is therefore typical to aim

to minimise bend-twist coupling, rather than eliminate it entirely.

The buckling constraint is satisfied following Stage II in all examples, however, the 1500 and 3000 με

examples violate strain constraints due to discrepancies between the target lamination parameters and those

achieved in the optimisation. These violations are not critical in this instance, as the purpose of the strain

allowables in this study is to generate a range of target lamination parameters. Converting from the continuous

lamination parameter optimisation problem to the discrete stacking sequence optimisation problem, results in

the strain constraint no longer being active in both examples d) and e). It is theoretically possible to decrease

thickness to violate the 4500 με constraint while satisfying the buckling constraint, as is achieved in the Stage I

result for example e) in Table 4, however, such a stack would have a non-integer number of plies. Examples d)

and e) are therefore interchangeable, as both satisfy constraints and have identical thickness. Such an outcome is

typical of stacking sequence design, wherein finding the "best" stack requires searching a multimodal design

space containing many possible solutions to the same design problem. It is emphasised that the results in Table

2 correspond to the best solution found by the genetic algorithm in this study, however, due to the stochastic

nature of this search method and the multimodal nature of the design space, these solutions are neither definitive

nor unique..

5.3. Blade-stiffened Panel

The second numerical example is a blade-stiffened wing panel, a more typical aerospace structure which is

commonly used as a benchmark problem for demonstrating optimisation methods [31,33,63,68]. Forming the

stiffeners from flat ply stacks could accelerate manufacture of such components, and is a potentially challenging

manufacturing problem. Rapid manufacture of wing skins, which are curved in practice, is also non-trivial. As

this paper contributes constraints on stacking sequence design, this example focusses upon optimising a panel

with fixed geometry. The model geometry and associated boundary conditions are illustrated in Figure 10.

For simplicity, the skin is assumed flat, and a single repeating unit of a wider panel is modelled by

exploiting symmetry planes located at the centre lines of two adjacent skin regions. Skin thickness t_{sk}, stiffener

thickness t_{st}, and the lamination parameters $\xi_{1,2}^{A,D}$ of both regions are varied in the optimisation. The stiffener is

assumed to be manufactured from two back-to-back L-sections with identical stacking sequence, resulting in a

stiffener blade with thickness $2t_{st}$. A longitudinal compressive force of $P_x = 1200$kN is applied as uniform edge

shortening, based upon a running load of 4kN/mm, consistent with a highly-stressed wing region. The panel is

clamped at the transverse edges. Symmetry is enforced by preventing rotation about the x axis at the

longitudinal edges of the repeating unit, which are constrained to be straight but free to expand, such that

transverse compression is not induced in the model. The latter condition assumes that, in the absence of shear

loading and significant bend-twist coupling, the skin modes are not skewed. Symmetry-enforcing boundary

conditions are taken from [42]. The skin and stiffener are meshed separately, and a tie constraint used to simulate bonding of the stiffener to this skin. The resulting mesh is composed of 6720 S4R quadrilateral shell elements, comprising 120 elements in the longitudinal direction, 38 elements across the skin width, and 6 elements across the stiffener flange and web widths, with an approximate element size of 8mm x 8mm throughout the model. This mesh was selected to achieve convergence of the first five buckling modes to three significant figures, while ensuring a minimum of five nodes per half-wavelength for each mode shape [63], as in the previous example. Note that doubling the number of elements across the stiffener web did not lead to a reduction in the first five buckling load factors at two significant figures.

In this optimisation, the cross-sectional area of the repeating unit is minimised, given by

$$A = bt_{sk} + (b_{st} + 2h_{st})t_{st} \tag{42}$$

This objective is minimised subject to buckling and strain constraints as in the previous example, using a longitudinal strain allowable of 4500 $\mu\varepsilon$. An additional constraint is applied in Stage I to ensure the skin to stiffener Poisson's ratio mismatch does not exceed 0.1, expressed as

$$\left| \frac{A_{12,st}}{A_{22.st}} - \frac{A_{12,sk}}{A_{22,sk}} \right| - 0.1 \leq 0 \tag{43}$$

where A_{12} and A_{22} are in-plane laminate stiffness as calculated using Eq. (20), and subscripts st and sk refer to properties of the stiffener and skin respectively.

Optimum lamination parameters and thicknesses in the stiffener and skin regions after both stages of the optimisation are shown in Table 5. Values of $\xi_4^{A,D}$ are omitted as these are automatically zero as previously stated. Resulting values of the first three buckling load factors, and limiting longitudinal strains are shown in Table 6, with the corresponding buckling modes illustrated in Figure 11. The damage tolerance constraint is only applied in the skin, as stiffeners are typically limited by edge-driven failure at the tip, to which the proposed method is not applicable. This constraint is evaluated by assuming a delamination arises in centre of the skin region, as illustrated in Figure 10. An applied strain of $\boldsymbol{\varepsilon} = \{-4234, 1822, 0\}^T$ is used in this constraint, taken from finite element model output of an element at this location. This strain is also shown in Table 6. The stacking sequences which result from Stage II of the optimisation are shown in Table 7 alongside key parameters of the formability and damage tolerance constraints.

Optimisation of the stiffeners in this example is driven primarily by strain, resulting in in-plane lamination parameters corresponding to the largest proportion of $0°$ plies permitted by the 10% rule, similar to the 1000 $\mu\varepsilon$ plate example. Design of the skin is driven primarily by buckling, with out-of-plane lamination parameter values corresponding to a large proportion of $\pm 45°$ plies on the outside of the laminate, with in-plane parameters ensuring there is sufficient stiffness to meet the strain constraint. A reasonable agreement is achieved in lamination parameter values between Stages I and II, in both the skin and stiffener, with the largest discrepancies arising in ξ_2^A and ξ_3^D of the skin. Balanced stacking sequences are achieved in both regions to match the target value of $\xi_3^A = 0$, unlike in the plate example.

All buckling constraints are met with significant margin following Stage II, due to the requirement of rounding the skin thickness to a discrete number of plies. The strain constraint is, however, not met following Stage II. This result occurs due to the small discrepancies in the achieved values of in-plane lamination parameters $\xi_{1,2}^A$ following Stage II, and the target values assumed due to the implementation of the 10% rule in Stage I, similar to those experienced in the plate examples. Specifically, the maximum proportion of $0°$ plies permitted in a 32-ply stack which satisfies the 10% rule is 62.5%, which is lower than the 70% proportion assumed during Stage I. As such, the stiffener is insufficiently stiff to meet the strain constraint, and in practice, additional $0°$ plies may be required . This result highlights a potential limitation of using a two-stage methodology alongside industrial design rules, in that the number of plies used in Stage II is determined based upon lamination parameter values which may not be feasible given this number of plies, and strict constraints imposed upon the stacking sequence. It is, however, emphasised that this result is not a direct consequence of the damage tolerance or C_{max} constraints.

6. DISCUSSION

In the above case studies, the damage tolerance and formability constraints are met, with a margin, for each of the optimised stacks. These designs were achieved while targeting a wide range of optimum lamination parameters corresponding to a variety of design criteria.

The minimum formability imposed by the C_{max} constraint is primarily achieved by limiting the number of $45°$ interfaces in the stack, within the restrictions of the contiguity and 10% rule constraints, as deformation mode compatibility is typically lower across these interfaces. By reducing the number of $45°$ interfaces, the

potential for in-plane shear to induce compressive forces in the fibres of adjacent plies during forming is minimised, and consequentially so is the likelihood of wrinkles occurring. The buckling-driven, ±45°-dominated stacks tend towards having two zones of orthogonal plies, with a zone of ±45° plies on the outside of stacks and a zone of 0°/90° plies in the centre. This zoned strategy reflects that used in the wrinkle-free specimens from the trials undertaken in [27], such as the example shown in Figure 7a). Examples of this zoned configuration include results of the plate optimisation with 3000-6000 µε strain allowable, and the skin of the stiffened panel. During forming, plies in each zone are free to deform in shear without restriction from interaction with stiff fibres in adjacent plies. Deformation between these zones would arise via slip at the 45/0 or -45/90 interface, as observed in the wrinkle-free examples of [27]. The ±45° zone in the skin of the stiffened panel is broken up with a single 0° ply, however, this exception is not sufficient to violate the formability constraint. It should be noted that there may be a set of more formable stacks which also achieve a good lamination parameter match. If necessary, these layups may be found by using a higher C_{max} target, which would likely result in more distinct zoning in this example.

A zoned formation does not arise in the more strain-driven designs, such as plate example a), and the stiffener laminate in the stiffened panel example. As there are a much larger number of 0° plies than 90° plies in these stacks, a single zone of 0° and 90° plies would violate the contiguity constraint. Instead, stacks are comprised of multiple 0/90° zones, and blocks of zeros interspersed with ±45° plies. The genetic algorithm orders these plies in such a way as to minimise the required number of slip planes without violating the contiguity constraint, thereby reducing the detrimental effect of the 45° interfaces upon forming.

There are two means by which damage tolerance is achieved in the case studies. When a low strain allowable is used in Stage I, applied strains are reduced such that damage tolerance is less critical to design. In plate example a), it is necessary to locate 0° plies on the outside of the laminate to match the target lamination parameters. While it is evident from Figure 9 that this configuration leads to low delamination propagation strains, the strain required to propagate the worst-case delamination, located at the 5th interface, is a factor of 1.87 higher than applied strains. When a higher strain allowable is used, ±45° plies are placed towards the outside of the stack, thereby increasing delamination propagation strains by redirecting stress away from these plies, increasing sub-laminate buckling strains, and reducing the strain energy stored in the sub-laminate by aligning fibres away from applied load. This configurations arises in the plate examples d) and e), in which a reserve factor of 1.45 is achieved relative to the strain required to propagate the worst-case delamination,

located at the 3rd interface (see Figure 9), and in the skin of the stiffened panel, in which a reserve factor of 1.02 is achieved. While these results conform to the common design practice of adding ±45° plies to the outside of laminates for damage tolerance, the proposed approach is advantageous in that it is mechanics-based rather than design rule-based, thereby ensuring the method is equally applicable to ply orientations other than 0, 90, and ±45°. Moreover, it may be noted that by increasing allowable strains in Table 3, reductions in thickness are achieved without violating the damage tolerance constraint. This observation highlights the limitations of current industrial practices employing fixed strain allowables, which do not account for the ability to impart greater damage tolerance by optimising the stacking sequence. It should be emphasised, however, that although rapid analytical models are necessary for their feasible inclusion in optimisation, the use of such simplified models should always be followed by detailed, high-fidelity modelling of more realistic damage morphologies and failure mechanisms, and testing at a damaged sub-component level or above, to verify the safety of resulting designs.

The number of sub-laminate buckling analyses required to evaluate the damage tolerance constraint, across the entire optimisation is typically in the orders of hundreds. Noting that a maximum of one analysis is required per ply (up to the laminate mid-plane), per candidate design, this result constitutes an order of two magnitudes reduction compared with a potential 30,000 sub-laminates, based upon a population size of 20 candidate designs with approximately 30 plies, run for 100 generations, thereby demonstrating the efficiency of the method.

Various strategies may be pursued to improve upon results by reducing the discrepancy between the target lamination parameters of the continuous Stage I optimum, and those which may be achieved by feasible stacking sequences in Stage II. Increasing the size of the feasible design space by extending the set of permissible ply orientations to include non-standard ply angles, or by relaxing the constraint upon symmetry, would increase the number of feasible designs in proximity to the target lamination parameters. The ply thickness of 0.25mm assumed in the numerical studies is particularly high, and use of thinner plies could also ensure a greater degree of flexibility for matching the target parameters.

The largest discrepancies arose due to the implementation of the 10% rule during Stage I, via the bounds defined in Section 4.1.3, which do not account for the fact that a larger proportion than 10% of each permissible ply orientation may be required to achieve an integer number of plies of each orientation. A more accurate set of bounds for this rule could be defined in lamination parameter space by directly accounting for the dependency upon both the laminate and ply thickness, to ensure that the bounding ply percentages correspond to an integer

number of plies. Definition of equivalent, potentially conservative expressions in lamination parameter space for the other constraints applied during Stage II may further reduce discrepancies, as was undertaken for manufacturing constraints associated with Variable Angle Tow laminates in [46] within the polar method. Such expressions may exist linking the sub-laminate in-plane lamination parameters to the lamination parameters of the parent laminate for the purpose of damage tolerance calculations. Due to its strong dependency upon stacking sequence [27], it is not anticipated that such expressions exist for the Compatibility Index.

7. CONCLUSIONS

In this paper, two new optimisation constraints have been proposed which enable simultaneous design for performance and manufacturability of composite aerospace structures. These constraints have been demonstrated within a two-stage optimisation framework to achieve minimum-mass designs, subject to buckling and strain constraints, as well as minimum targets on damage tolerance and formability. A new damage tolerance constraint ensures applied strains do not exceed a predicted lower bound on the strain required to propagate a delamination, given any through-thickness delamination position and an upper bound on delamination size. A new manufacturing constraint enforces a minimum stack formability, using a compatibility index to predict the tendency of wrinkles to arise during forming of ply stacks using high-rate processes, calculated using an efficient linear integer programming method.

Across case studies considering a range of design criteria, buckling constraints were met in all examples, however, limitations imposed by existing composite design rules led to some violations of strain constraints after practical stacking sequence design. Both new constraints were met, with a margin, in all examples. The damage tolerance constraint was typically met by locating ±45° on the outside of stacks. This result corresponds with current design practice but also provides a figure of merit which may be applied to non-standard ply angles in future work. The formability constraint was met by grouping plies into mutually orthogonal 0/90° or ±45° zones, minimising 45° interfaces where possible, to promote shear during forming while reducing the potential for compressive stresses to arise in fibres, leading to wrinkling.

Noting that the formability constraint was met without increasing mass or reducing buckling loads, these case studies have demonstrated that design for manufacturability may potentially be achieved without detriment to performance. The fact that these qualities need not be mutually exclusive is an encouraging outcome which

31

highlights the possibility for manufacture of high-performance, lightweight composite aircraft components using high-rate processes.

ACKNOWLEDGEMENTS

REFERENCES

[1] X.C. Sun, S.R. Hallett. Failure mechanisms and damage evolution of laminated composites under compression after impact (CAI): Experimental and numerical study. Compos. Part A Appl. Sci. Manuf. 104 (2018) 41–59.

[2] M.R. Abir, T.E. Tay, M. Ridha, H.P. Lee. Modelling damage growth in composites subjected to impact and compression after impact. Compos. Struct. 168 (2017) 13–25.

[3] W. Tan, B.G. Falzon, L.N.S. Chiu, M. Price. Predicting low velocity impact damage and Compression-After-Impact (CAI) behaviour of composite laminates. Compos. Part A Appl. Sci. Manuf. 71 (2015) 212–26.

[4] R. Borrelli, A. Riccio, A. Sellitto, F. Caputo, T. Ludwig. On the use of global–local kinematic coupling approaches for delamination growth simulation in stiffened composite panels. Compos Sci Technol 115 (2015) 43–51.

[5] H. Chai, C.D. Babcock, W.G. Knauss. One dimensional modelling of failure in laminated plates by delamination buckling. Int. J. Solids Struct. 17 (1981) 1069–83.

[6] H. Chai, C.D. Babcock. Two-Dimensional Modelling of Compressive Failure in Delaminated Laminates. J. Compos. Mater. 19 (1985) 67–98.

[7] J.W. Hutchinson, Z. Suo. Mixed Mode Cracking in Layered Materials. Adv. Appl. Mech, 29 (1991) 63–191.

[8] R. Butler, A.T. Rhead, W. Liu, N. Kontis. Compressive strength of delaminated aerospace composites. Philos. Trans. R. Soc. A Math. Phys. Eng. Sci. 370 (2012) 1759–79.

[9] A.T. Rhead, R. Butler. Compressive static strength model for impact damaged laminates. Compos. Sci.

Technol. 69 (2009) 2301–7.

[10] R.S. Choudhry, A.T. Rhead, M.W.D. Nielsen, R. Butler. A plate model for compressive strength prediction of delaminated composites. Compos. Struct. 210 (2019) 509–17.

[11] F.W. Williams, D. Kennedy, R. Butler, M.S. Anderson. VICONOPT - Program for exact vibration and buckling analysis or design of prismatic plate assemblies. AIAA J. 29 (1991) 1927–8.

[12] A. Köllner, F. Forsbach, C. Völlmecke. Delamination buckling in composite plates: an analytical approach to predict delamination growth. In: B.E. Abali, H. Altenbach, F. dell'Isola, V.A. Eremeyev, A. Öchsner, editors. New Achievements in Continuum Mechanics and Thermodynamics. Vol. 108 of Advanced Structured Materials, Springer, 2019, p. 241–55.

[13] A. Köllner, M.W.D. Nielsen, J. Srisuriyachot, A.T. Rhead, R. Butler. Buckle-driven delamination models for laminate strength prediction and damage tolerant design. Thin-Walled Struct. 161 (2021).

[14] A. Riccio, P. Perugini, F. Scaramuzzino. Modelling compression behaviour of delaminated composite panels. Comput. Struct. 78 (2000):73–81.

[15] J. Sjölander, P. Hallander, M. Åkermo. Forming induced wrinkling of composite laminates: A numerical study on wrinkling mechanisms. Compos. Part A Appl. Sci. Manuf. 81 (2016) 41–51.

[16] S.P. Haanappel, R.H.W. ten Thije, U. Sachs, B. Rietman, R. Akkerman. Formability analyses of uni-directional and textile reinforced thermoplastics. Compos. Part A Appl. Sci. Manuf. 56 (2014) 80–92.

[17] X.X. Bian, Y.Z. Gu, J. Sun, M. Li, W.P. Liu, Z.G. Zhan. Effects of Processing Parameters on the Forming Quality of C-Shaped Thermosetting Composite Laminates in Hot Diaphragm Forming Process. Appl. Compos. Mater. 20 (2013) 927–45.

[18] P. Hallander, J. Sjölander, M. Petersson, M. Åkermo. Interface manipulation towards wrinkle-free forming of stacked UD prepreg layers. Compos. Part A Appl. Sci. Manuf. 90 (2016) 340–8.

[19] P. Hallander, M. Akermo, C. Mattei, M. Petersson, T. Nyman. An experimental study of mechanisms behind wrinkle development during forming of composite laminates. Compos. Part A Appl. Sci. Manuf. 50 (2013) 54–64.

[20] P. Hallander, J. Sjölander, M. Åkermo. Forming induced wrinkling of composite laminates with mixed ply material properties; an experimental study. Compos. Part A Appl. Sci. Manuf. 78 (2015) 234–45.

[21] H. Alshahrani, M. Hojjati. Experimental and numerical investigations on formability of out-of-autoclave thermoset prepreg using a double diaphragm process,. Compos. Part A Appl. Sci. Manuf. 101 (2017) 199–

1   214.

2   [22] C. Mack, H.M. Taylor. The Fitting of Woven Cloth to Surfaces, J. Text. Inst. 47 (1956) T477–88.

3   [23] R.H.W. ten Thije, R. Akkerman, J. Huétink. Large deformation simulation of anisotropic material using an

4   updated Lagrangian finite element method. Comput. Methods Appl. Mech. Eng. 196 (2007) 3141–50.

5   [24] P. de Luca, P. Lefébure, A.K. Pickett. Numerical and experimental investigation of some press forming

6   parameters of two fibre reinforced thermoplastics: APC2-AS4 and PEI-CETEX, Compos. Part A Appl. Sci.

7   Manuf. 29 (1998) 101–10.

8   [25] K. Vanclooster, S.V. Lomov, I. Verpoest. Experimental validation of forming simulations of fabric

9   reinforced polymers using an unsymmetrical mould configuration. Compos. Part A Appl. Sci. Manuf. 40

10   (2009) 530–9.

11   [26] D. Dörr, W. Brymerski, S. Ropers, D. Leutz, T. Joppich, L. Kärger. A Benchmark Study of Finite Element

12   Codes for Forming Simulation of Thermoplastic UD-Tapes, Procedia CIRP 66 (2017) 101–6.

13   [27] K.J. Johnson, R. Butler, E.G. Loukaides, C. Scarth, A.T. Rhead. Stacking sequence selection for defect-free

14   forming of uni-directional ply laminates, Compos. Sci. Technol. 171 (2019) 34-43.

15   [28] H. Ghiasi, D. Pasini, L. Lessard. Optimum Stacking Sequence Design of Composite Materials Part I:

16   Constant Stiffness Design. Compos. Struct. 90 (2009) 1–11.

17   [29] R. Le Riche, R.T. Haftka. Optimization of Laminate Stacking Sequence for Buckling Load Maximization

18   by Genetic Algorithm. AIAA J. 31 (1993) 951–6.

19   [30] K.J. Callahan, G.E. Weeks. Optimum Design of Composite Laminates using Genetic Algorithms. Compos.

20   Eng. 2 (1992) 149–60.

21   [31] C. Bisagni, L. Lanzi. Post-buckling optimisation of composite stiffened panels using neural networks.

22   Compos. Struct. 58 (2002) 237–47.

23   [32] C. Bisagni, R. Vescovini. A fast procedure for the design of composite stiffened panels. Aeronaut. J. 119

24   (2015) 185–201.

25   [33] S. Nagendra, D. Jestin, Z. Gürdal, R.T. Haftka, L.T. Watson. Improved genetic algorithm for the design of

26   stiffened composite panels. Comput. Struct. 58 (1996) 543–55.

27   [34] S.W. Tsai, J.C. Halpin, N.J. Pagano. Composite Materials Workshop, Technomic, Stamford, Conn. 1968.

28   [35] S.W. Tsai, H.T. Hahn HT. Introduction to Composite Materials. Lancaster, PA: Technomic, 1980.

29   [36] M. Miki. Material design of composite laminates with required in-plane elastic properties. In: T. Hayashi,

1   K. Kawata, S, Umekawa, editors, Progress in Science and Engineering in composites. Proceedings of the

2   4th International Conference on Composite Materials (ICCM IV), Tokyo, 1982, p. 1727-31.

3   [37] M. Miki, Y. Sugiyama. Optimum Design of Laminated Composite Plates Using Lamination Parameters.

4   AIAA J. 31 (1993) 921–2.

5   [38] H. Fukunaga, H. Sekine. Stiffness Design Method of Symmetric Laminates using Lamination Parameters.

6   AIAA J. 30 (1992) 2791–3.

7   [39] H. Fukunaga, G.N. Vanderplaats. Stiffness Optimization of Orthotropic Laminated Composites Using

8   Lamination Parameters. AIAA J. 29 (1991) 641–6.

9   [40] K. Yamazaki. Two-level optimization technique of composite laminate panels by genetic algorithms. In:

10   Proceedings of the 37th Structures, Structural Dynamics and Materials Conference, AIAA, 1996.

11   [41] A. Todoroki, R.T. Haftka. Stacking sequence optimization by a genetic algorithm with a new recessive

12   gene like repair strategy. Compos. Part B Eng. 29 (1998) 277–85.

13   [42] J.E. Herencia, P.M. Weaver, M.I. Friswell. Optimization of long anisotropic laminated fiber composite

14   panels with T-shaped stiffeners. AIAA J. 45 (2007) 2497–509.

15   [43] M.A. Albazzan, R. Harik, B.F. Tatting, Z. Gürdal. Efficient design optimization of nonconventional

16   laminated composites using lamination parameters: A state of the art. Compos. Struct. 209 (2019) 362–74.

17   [44] P. Vannucci, G. Verchery. Stiffness design of laminates using the polar method. Int. J. Solids Struct. 38

18   (2001) 9281–94.

19   [45] P. Vannucci, G. Verchery. A special class of uncoupled and quasi-homogeneous laminates. Compos. Sci.

20   Technol. 61 (2001) 1465–73.

21   [46] M. Montemurro, A. Catapano. On the effective integration of manufacturability constraints within the

22   multi-scale methodology for designing variable angle-tow laminates. Compos. Struct. 161 (2017) 145–59.

23   [47] M. Montemurro, A. Pagani, G.A. Fiordilino, J. Pailhès, E. Carrera. A general multi-scale two-level

24   optimisation strategy for designing composite stiffened panels. Compos. Struct. 201 (2018) 968–79.

25   [48] M. Montemurro, M.I. Izzi, J. El-Yagoubi, D. Fanteria. Least-weight composite plates with unconventional

26   stacking sequences: Design, analysis and experiments. J. Compos Mater. 53 (2019) 2209–27.

27   [49] M.I. Izzi, M. Montemurro, A. Catapano, J. Pailhès. A multi-scale two-level optimisation strategy

28   integrating a global/local modelling approach for composite structures. Compos. Struct. 237 (2020).

29   [50] D. Hull, Y.B. Shi. Damage mechanism characterization in composite damage tolerance investigations.

Compos. Struct. 23 (1993) 99–120.

[51] W.H. Wittrick, F.W. Williams. A general algorithm for computing natural frequencies of elastic structures. Q. J. Mech. Appl. Math. 24 (1971) 263–84.

[52] M.S. Anderson, F.W. Williams, C.J Wright. Buckling and vibration of any prismatic assembly of shear and compression loaded anisotropic plates with an arbitrary supporting structure. Int. J. Mech. Sci. 25 (1983) 585–96.

[53] A.T. Rhead, R. Butler, N. Baker. Analysis and compression testing of laminates optimised for damage tolerance. Appl. Compos. Mater. 18 (2011) 85–100.

[54] ASTM Standard D7136. Standard Test Method for Measuring the Damage Resistance of a Fiber-Reinforced Polymer Matrix Composite to a Drop-Weight Impact Event. Book of Standards, Vol. 15.03, 2005.

[55] W. Thomson. Elements of a Mathematical Theory of Elasticity. Philos. Trans. R. Soc. London 146 (1856) 481–98.

[56] M.M. Mehrabadi, S.C. Cowin. Eigentensors of linear anisotropic elastic materials. Q. J. Mech. Appl. Math. 43 (1990) 15–41.

[57] MATLAB R2019a, The MathWorks Inc. Natick, Massachusetts, USA, 2019.

[58] C.G. Diaconu, H. Sekine. Layup Optimization for Buckling of Laminated Composite Shells with Restricted Layer Angles. AIAA J. 42 (2004) 2153–63.

[59] M. Abdalla, Z. Gurdal, C. Kassapoglu. Formulation of Composite Laminate Robustness Constraint in Lamination Parameters Space. In: Proceedings of the 50th AIAA/ASME/ASCE/AHS/ASC Structures, Structural Dynamics and Materials Conference, AIAA, 2009.

[60] B. Liu B, R.T. Haftka, P. Trompette. Maximization of buckling loads of composite panels using flexural lamination parameters. Struct. Multidiscip. Optim. 26 (2004) 28–36.

[61] L.E. Culliford, C. Scarth, T. Maierhofer, R. Jagpal, A.T. Rhead, R. Butler. Discrete Stiffness Tailoring: Optimised design and testing of minimum mass stiffened panels. Compos .Part B Eng. 221 (2021).

[62] C. Scarth, J.E. Cooper. Reliability-based aeroelastic design of composite plate wings using a stability margin. Struct. Multidiscip. Optim. 57 (2018) 1695-1709.

[63] J.E. Herencia, P.M. Weaver, M.I. Friswell. Optimization of Anisotropic Composite Panels with T-shaped Stiffeners Including Transverse Shear Effects and Out-of-Plane Loading. Struct. Multidiscip. Optim. 37

1   (2008) 165–84.

2   [64] ABAQUS 6.14-2. Dassault Systèmes, Providence, RI, USA, 2014.

3   [65] K. Deep, K.P. Singh, M.L. Kansal, C. Mohan. A real coded genetic algorithm for solving integer and mixed

4   integer optimization problems. Appl. Math. Comput. 212 (2009) 505–18.

5   [66] T.J. Dodwell, R. Butler, A.T. Rhead. Optimum Fiber Steering of Composite Plates for Buckling and

6   Manufacturability. AIAA J. 54 (2016) 1146–9.

7   [67] Abaqus Analysis User's Guide, Version 6.14. Dassault Systèmes Simulia Corp., Providence, RI, USA,

8   2014.

9   [68] W. Liu, R. Butler, A.R. Mileham, A.J. Green. Bilevel optimization and postbuckling of highly strained

10   composite stiffened panels. AIAA J. 44 (2006) 2562–70.

11   [69] T.R.C. Chuaqui, M.W.D. Nielsen, J. Colton, R. Butler, A.T. Rhead. Effects of ply angle and blocking on

12   open-hole tensile strength of composite laminates: A design and certification perspective. Compos. Part B
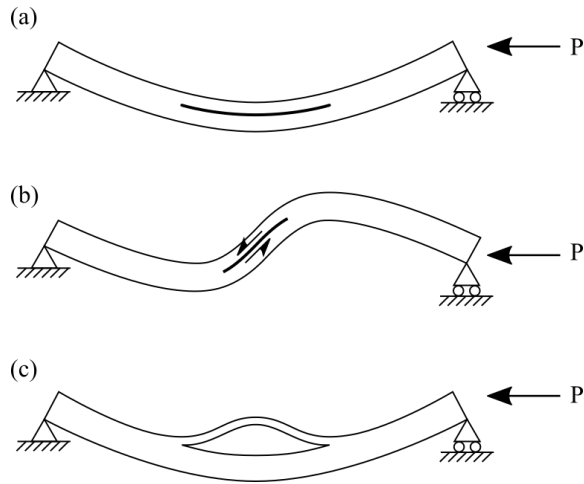
13   Eng. 207 (2021).

14

Figure 1. Post-buckling modes of delaminated plates: a) symmetric closing, b) antisymmetric closing (and shearing) and c) symmetric opening.
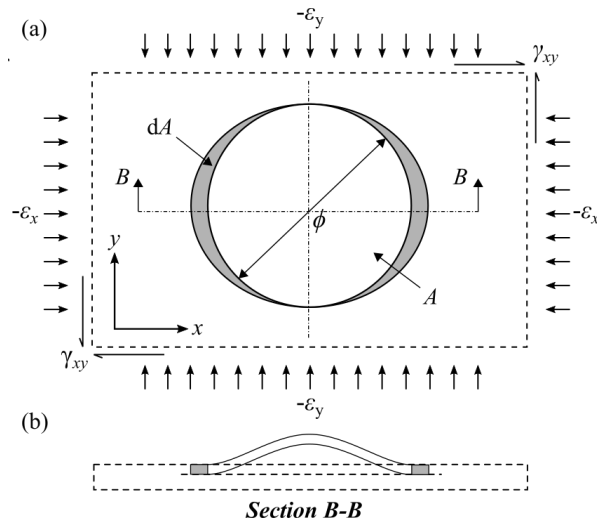

Figure 2. Idealised post-buckled geometry and propagation of delamination. a) Plan view of circular delamination area b) section B-B of geometry.

(a)

START

Initialise:
$F_{th,lb} = \infty$
$i = 1$

Determine
$F_{th,i}$
(see detail)

Next ply
interface:
$i = i + 1$

Is
$F_{th,i} \leq F_{th,lb}$?

NO

YES

$F_{th,lb} = F_{th,i}$

Are stopping
criteria met?

NO

YES

STOP

(b)

Determine $F_{th,i}$

START

Is
$F_{th,min} \geq 1$?
Eq.(5)

YES

NO

Determine F_C
for $\phi = \phi_{max}$
(VICONOPT)

Is
$F_C \leq F_{th,min}/3$?

YES

$F_{th,i} = F_{th,min}$
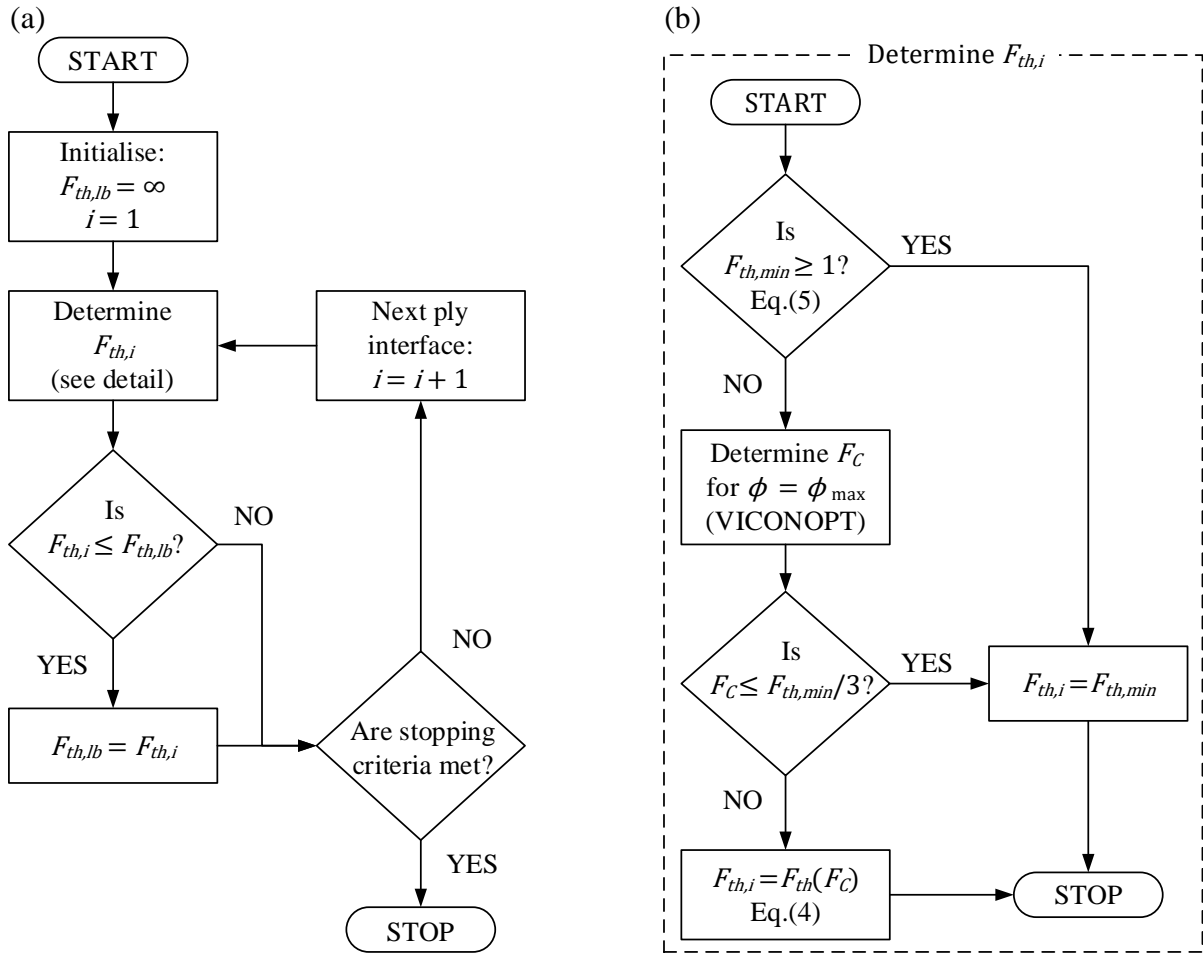
NO

$F_{th,i} = F_{th}(F_C)$
Eq.(4)

STOP

Figure 3. Algorithm for finding delamination propagation strain lower bound. a) outer loop searching over ply

interfaces b) inner subroutine determining propagation strain for a delamination at a given interface.
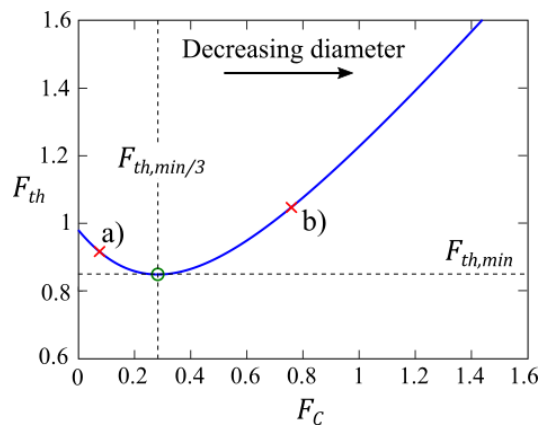

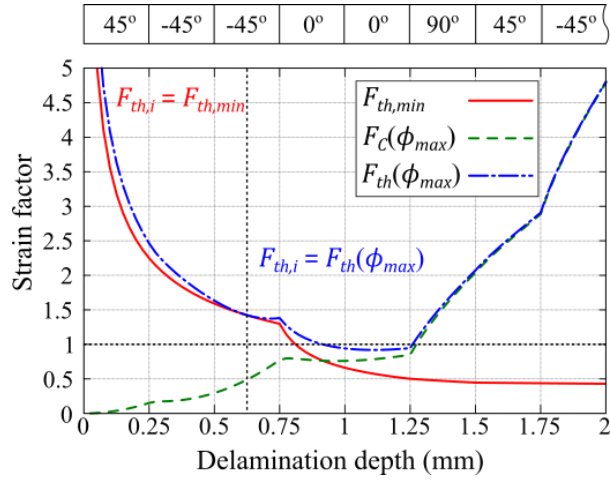Figure 4.Threshold strain factor trends with respect to sub-laminate buckling factor.

45°	-45°	-45°	0°	0°	90°	45°	-45°

Figure 5. Strain factor trends with increasing delamination depth for outer stacking sequence

$[45 /\text{-}45_2/0_2/90/\pm45/...]$, applied strain $\boldsymbol{\varepsilon} = \{-4500, 3500, 0\}^T \mu\varepsilon$, and $\phi_{max} = 50$mm.

Transverse Mode 1   Shear Mode 2/2*   Fibre Mode 3

$\boldsymbol{v}_1 = [0, 1, 0]$ $\boldsymbol{v}_2 = [0, 0, 1]$ $\boldsymbol{v}_{2^*} = [0, 0, -1]$ $\boldsymbol{v}_3 = [1, 0, 0]$
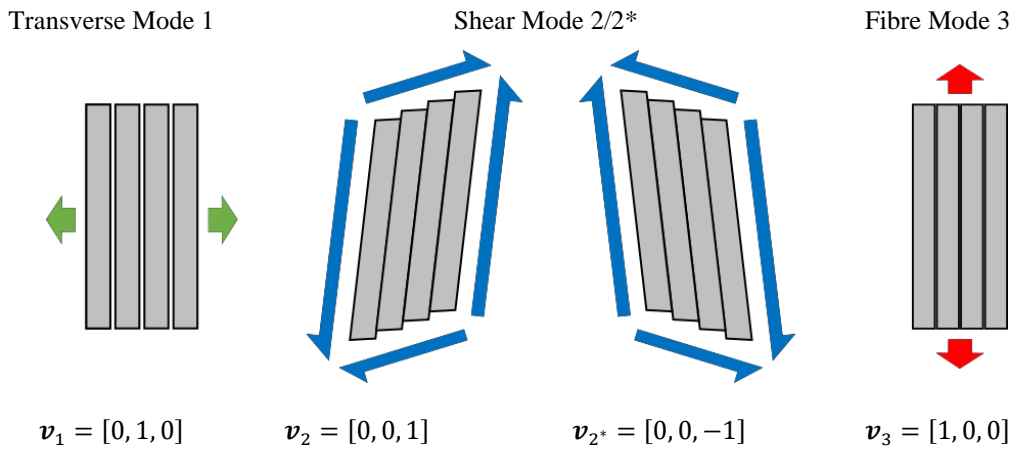
Figure 6. Independent ply deformation modes for single 0° uncured ply [27].

1

Cured part	C_{max}
a) $[(\pm45)/(0/90)_3]_S$	
	0.91
b) $[(45/0)_3/(-45/90)_3]_S$	
	0.70
c) $[(45/0/-45/90)_3]_S$	
	0.56

1   Figure 7. Web outer (non-tool) surface view of cured C-spars manufactured in the Double Diaphragm

2   Forming trials from [27], demonstrating correlation of the severity of wrinkles with lower values of C_{max}.
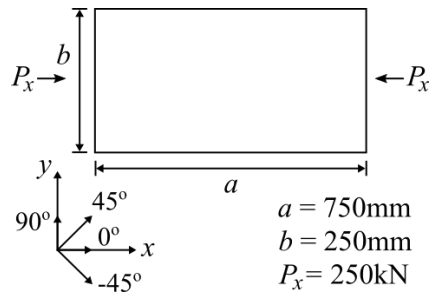

Figure 8. Model definition for flat plate example.

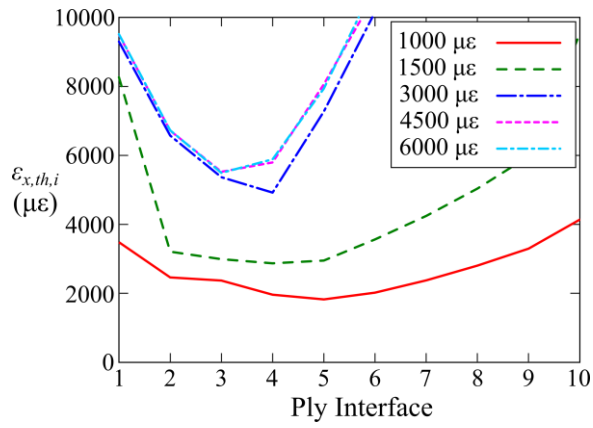Figure 9. Lower bound delamination propagation strain at each ply interface, for a range of target strains.
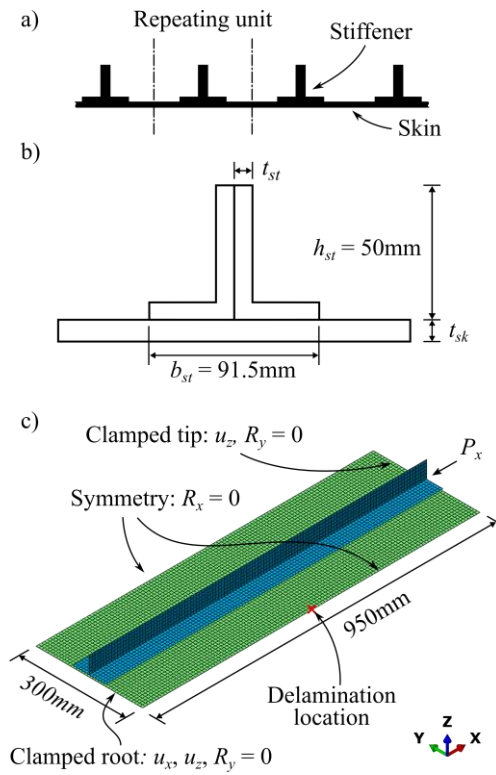

Figure 10. Stiffened panel geometry and boundary conditions: a) illustration of model context within wider

panel, b) panel cross sectional geometry, c) finite element model highlighting boundary conditions.
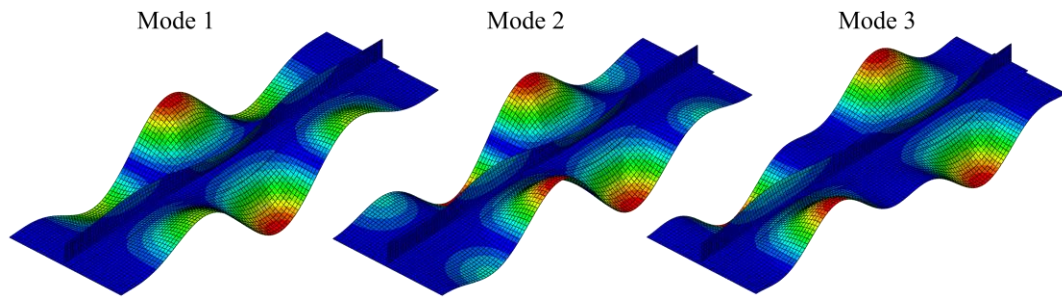
Mode 1   Mode 2   Mode 3

Figure 11. First three buckling modes of optimised panel.

Table 1. Experimental and analytical delamination propagation strains (in microstrain). Analytical strains are obtained at various ply interfaces, *i,* from the back (non-impact) face using: a) C-scan data and b) constant circular delamination of diameter $\phi_{max} = 36$mm, with $G_{IC} = 300$ J/m^2 and $G_{IIC} = 870$ J/m^2 [69].

Laminate	Experimental propagation strain [53]	a) ϕ_{max} taken from C-scan data			b) ϕ_{max} = 36 mm	
		Analytical buckling strain (at interface *i*)	Analytical propagation strain (at interface *i*)		Analytical propagation strain (at interface *i*)	
			$G_C = G_{IC}$	$G_C = G_{IIC}$	$G_C = G_{IC}$	$G_C = G_{IIC}$
Control	5700	1796 (2) 3446 (3) 3709 (4)	3523 (2) 4335 (3) 4463 (4)	5788 (2) 5791 (3) 5732 (4)	2971 (4)	4762 (6)
±45° Outer	5900 – 7400	1904 (2) 5874 (3)	5670 (2) 7033 (3)	9878 (2) 8987 (3)	4063 (4)	6258 (5)
90° Outer	6400 (Test1) 6200 (Test2)	807 (3) 3014 (4)	5515 (3) 4959 (4)	9727 (3) 7725 (4)	5689 (4)	8029 (4)

Table 2. Optimised stacking sequence for a range of target strain values.

	Target Strain (µε)	Stacking sequence
a)	1000	[0$_2$/90/0$_2$/-45/0$_3$/45/0/45/0$_2$/-45/0$_2$/90/0$_2$]$_S$
b)	1500	[-45/0/-45/45$_2$/0$_4$/90/0/90/0$_2$]$_S$
c)	3000	[-45/45$_3$/-45/45/-45$_2$/90/0$_2$/90/0]$_S$
d)	4500	[(±45)$_4$/-45/(90/0)$_2$]$_S$
e)	6000	[45/-45$_2$/±45/45$_2$/-45$_2$/(0/90)$_2$]$_S$

Table 3. Optimised lamination parameters and laminate thickness achieved during Stages I and II of the optimisation for a range of target strain values.

	Stage I							Stage II						
	ξ_1^A	ξ_2^A	ξ_3^A	ξ_1^D	ξ_2^D	ξ_3^D	*t* (mm)	ξ_1^A	ξ_2^A	ξ_3^A	ξ_1^D	ξ_2^D	ξ_3^D	*t* (mm)
a)	0.6	0.6	0.0	0.556	0.697	0.0	9.77	0.6	0.6	0.0	0.607	0.683	-0.022	10.00
b)	0.554	0.509	0.0	0.337	-0.140	0.0	6.85	0.429	0.429	0.0	0.378	-0.127	-0.125	7.00
c)	0.156	-0.288	0.0	0.037	-0.910	0.0	6.47	0.077	-0.231	0.0	-0.005	-0.886	0.120	6.50
d)	0.012	-0.577	0.0	0.001	-0.981	0.0	6.44	0.0	-0.385	-0.077	-0.011	-0.942	0.071	6.50
e)	0.0	-0.6	0.0	0.0	-0.983	0.0	6.44	0.0	-0.385	-0.077	0.011	-0.942	-0.028	6.50

Table 4. Constraint values following optimisation Stages I and II for a range of target strain values.

| | Stage I | | Stage II | | | | | |
| | Laminate buckling load factor | Longitudinal strain (με) | Laminate buckling load factor | Longitudinal strain (με) | Damage Tolerance | | | C_{max} |
					$\varepsilon_{x,th,lb}$ (με)	$F_{th,lb}$	N_{runs}	
a)	2.09	1000	2.17	976.6	1825	1.87	314	0.86
b)	1.00	1500	1.03	1624	2872	1.76	650	0.88
c)	1.00	3000	1.00	3106	4921	1.58	487	0.92
d)	1.00	4500	1.02	3789	5524	1.45	362	0.92
e)	1.00	4686	1.02	3789	5492	1.45	253	0.92

Table 5. Optimised lamination parameters and laminate thickness in skin and stiffener regions, achieved during

Stages I and II of the stiffened panel optimisation.

| Stage | Skin | | | | | | | Stiffener | | | | | | |
	ξ_1^A	ξ_2^A	ξ_3^A	ξ_1^D	ξ_2^D	ξ_3^D	t_{sk} (mm)	ξ_1^A	ξ_2^A	ξ_3^A	ξ_1^D	ξ_2^D	ξ_3^D	t_{st} (mm)
I	0.226	-0.015	0.0	0.047	-0.761	0.0	7.01	0.588	0.579	0.0	0.310	-0.006	0.0	7.99
II	0.172	-0.103	0.0	0.066	-0.765	0.171	7.25	0.500	0.500	0.0	0.380	0.137	-0.070	8.00

Table 6. Buckling load factor of the first three buckling modes, limiting longitudinal strains, achieved during

Stages I and II of the stiffened panel optimisation.

	F_1	F_2	F_3	Maximum strain (με)	Delamination location strain (με)
Stage I	1.00	1.00	1.07	4500	4234
Stage II	1.07	1.07	1.15	4815	4517

Table 7. Optimised stacking sequences and associated formability and damage tolerance constraint values (MS

denotes a symmetric laminate with odd number of plies, with mid-plane in the central 0° ply).

| | Stacking Sequence | C_{max} | Damage Tolerance | |
			$\varepsilon_{x,th,lb}$ (με)	$F_{th,lb}$
Skin	[45_2/-45/45/-45_2/0/±45/90/0_3/90/0]$_{MS}$	0.89	4624	1.02
Stiffener	[±45/0_2/-45/0_2/90_2/0_4/45/0_2]$_S$	0.86	N/A	N/A

1